Biomedicine & Pharmacotherapy 153 (2022) 113283

Contents lists available at ScienceDirect

Biomedicine & Pharmacotherapy

journal homepage: www.elsevier.com/locate/biopha

Ecklonia cava extracts decrease hypertension-related vascular calcification by modulating PGC-1α and SOD2

Kyung-A Byun [a,b,1], Seyeon Oh [b,1], Jin Young Yang [b], So Young Lee [c], Kuk Hui Son [c,*], Kyunghee Byun [a,b,**]

[a] Department of Anatomy & Cell Biology, Gachon University College of Medicine, Incheon 21936, Republic of Korea
[b] Functional Cellular Networks Laboratory, Lee Gil Ya Cancer and Diabetes Institute, Gachon University College of Medicine, Incheon 21999, Republic of Korea
[c] Department of Thoracic and Cardiovascular Surgery, Gachon University Gil Medical Center, Gachon University, Incheon 21565, Republic of Korea

ARTICLE INFO

Keywords:
Peroxisome proliferator-activated receptor-gamma coactivator-1 alpha
Sirtuin-3
Superoxide dismutase 2
Mitochondrial reactive oxygen species
Ecklonia cava extract

ABSTRACT

Vascular calcification (VC) is induced by a decrease in sirtuin 3 (SIRT3) and superoxide dismutase (SOD)2 and increases mitochondrial reactive oxygen species (mtROS), eventually leading to mitochondrial dysfunction and phenotype alterations in vascular smooth muscle cells (VSMCs) into osteoblast-like cells in hypertension. *Ecklonia cava* extract (ECE) is known to increase peroxisome proliferator-activated receptor-gamma coactivator-1 alpha (PGC-1α) and SOD2. In this study, we evaluated the effect of ECE on decreasing VC by increasing PGC-1α which increased SOD2 activity and decreased mtROS in an in vitro VSMC model of treating serums from Wistar Kyoto (WKY), spontaneous hypertensive rats (SHRs), and ECE-treated SHRs. Furthermore, the decreasing effect of ECE on VC was evaluated with an in vivo SHR model. PGC-1α expression, SIRT3 expression, and SOD2 activity were decreased by the serum from the SHRs and increased by the serum from the ECE-treated SHRs in the VSMCs. PGC-1α silencing eliminated those increases. mtROS generation and mitochondrial DNA (mtDNA) damage increased in the SHRs but decreased with ECE. Mitochondrial fission increased in the SHRs but decreased by ECE. Mitochondrial fusion, mitophagy, and mitochondrial biogenesis were decreased in the SHRs but increased by ECE. Nicotinamide adenine dinucleotide phosphate (NADPH) oxidase and calcium deposition in the medial layer of the aorta increased in the SHRs but decreased with ECE. Therefore, ECE decreases VC via the upregulation of PGC-1α and SIRT3, which increases SOD2 activity. Activated SOD2 decreases mtDNA damage and mtROS generation, which sequentially decreases NADPH oxidase activity and changes the mitochondrial dynamics, thereby decreasing VC.

1. Introduction

Vascular calcification (VC) is a mineral deposition that generally takes the form of calcium phosphate complexes in the vascular system [1]. VC is frequently accompanied by diabetes, hypertension, and chronic kidney disease and is also involved in the progression of these diseases [1]. VC is not only associated with pathological conditions but also with normal aging [1].

VC calcification can be classified into two types, depending on the site of the mineral deposition in the blood vessels: intimal and medial. Intimal calcification exhibits mineral depositions that are mainly in the intimal layer and is more related to lipid deposits and the infiltration of inflammatory cells [2]. Intimal calcification is usually accompanied by obstructive arterial disease, including coronary artery disease. However, medial calcification is more related to the transformation of vascular smooth muscle cells (VSMC) into osteoblast-like cells. Medial calcification tends to manifest more in hypertension or diabetes and causes arterial stiffness rather than obstruction [2].

Arterial stiffness is positively associated with cardiovascular mortality [3]. Various factors are involved in the pathophysiology of VC, such as inflammatory cytokines, changes in lipid metabolism, and excessive oxidative stress [4]. Oxidative stress, which originates from an imbalance between antioxidants and reactive oxygen species (ROS), promotes VSMC phenotype changes that result in them transforming

* Corresponding author.
** Corresponding author at: Department of Anatomy & Cell Biology, Gachon University College of Medicine, Incheon 21936, Republic of Korea.
E-mail addresses: dr632@gilhospital.com (K.H. Son), khbyun1@gachon.ac.kr (K. Byun).
[1] These authors contributed equally to this work.

https://doi.org/10.1016/j.biopha.2022.113283
Received 29 November 2021; Received in revised form 5 June 2022; Accepted 8 June 2022
Available online 16 June 2022

into osteoblast-like cells and that trigger apoptosis [5–7]. Osteoblast-like cells lead to increased mineral deposition due to the increased expression of bone morphogenetic protein 2 (BMP2), runt-related transcription factor 2 (RUNX2), Msh Homeobox 2, and osterix [8–11].

Hypertension might be involved in the development of VC since any fluctuations in blood pressure (BP) lead to changes in adenosine triphosphate (ATP) production, the promotion of ROS generation, and mitochondrial dysfunction in VSMCs. BP fluctuations also lead to mitochondrial reorganization by altering mitochondrial fission and fusion proteins, such as mitofusins (MFNs), mitochondrial optic atrophy protein 1 (OPA1), and dynamin-related protein 1 (DRP1) [12]. The mitochondrial fission and fusion alternations that are induced by increased oxidative stress are also related to VC [13]. Moreover, mitochondrial dysfunction results in the impairment of adequate ATP generation, decreased cellular viability, decreased mitochondrial protein synthesis, and mitophagy alterations. Mitochondrial dysfunction is also caused by increased mitochondrial ROS (mtROS) generation and mitochondrial DNA (mtDNA) damage [14].

Manganese superoxide dismutase 2 (SOD2), a main antioxidant enzyme in mitochondria, eliminates free radicals and protects cells from oxidative stress [15,16]. SOD2 activity decreases due to acetylation [17,18]. Mitochondrial sirtuin 3 (SIRT3), which is a nicotinamide adenine dinucleotide–dependent mitochondrial protein deacetylase, leads to SOD2 deacetylation at lysine 68 and increases SOD2 activity [17,19]. SOD2 that has been upregulated due to SIRT3 modulation leads to decreased mtROS and attenuated VSMC calcification [20]. However, SIRT3 inhibition results in increased VSMC calcification [20].

Peroxisome proliferator-activated receptor-gamma coactivator-1 alpha (PGC-1α) is a key endogenous activator of SIRT3 and is involved in decreasing VC by increasing SOD2 [20]. The overexpression of PGC-1α leads to SOD2 upregulation and decreased mtROS generation and thus inhibits VSMC migration and decreased neointima formation [21]. PGC-1α is a transcriptional coactivator of nuclear factor erythroid 2–related factor2 (NRF2) and estrogen receptor–related receptor alpha (ERRα) [22–25]. In addition, PGC-1α interacts with NFR2 and binds to the promoter of SIRT3, which consequently increases SIRT3 transcription [26].

Ecklonia cava is an edible brown alga that mainly grows in Korea and Japan [27]. *Ecklonia cava* extract (ECE), which is enriched in various polyphenols, primarily phlorotannins, shows many biological activities [28,29]. The polyphenols in ECE decrease oxidative stress by increasing NRF2 and SOD2 and decrease obesity-induced renal inflammation by increasing renal SIRT1, PGC-1α, and adenosine monophosphate (AMP)-activated protein kinase (AMPK) expression [30].

Although studies have shown that ECE has antioxidant effects via NRF2, SOD2, and PGC-1α modulation, whether ECE attenuates VC by modulating PGC-1α/NFR2/SIRT3, which leads to increasing SOD2 activity and mitochondrial function in hypertension, is unclear. We evaluated the effect of ECE on increasing PGC-1α/NFR2/SIRT3 and decreasing mitochondrial dysfunction by reducing mtROS generation and mtDNA damage and thus decreasing the osteoblast-like phenotype changes in VSMCs and medial calcification in the aortas of spontaneous hypertensive rats (SHRs).

2. Materials and methods

2.1. Preparation of ECE

Ecklonia cava was obtained from Aqua Green Technology Co., Ltd. (Jeju, Korea). For extraction, *Ecklonia cava* was washed and air-dried at room temperature for 48 h. It was then ground, and 50% ethanol was added, followed by incubation at 85 °C for 12 h. The *Ecklonia cava* extract (ECE) was filtered, concentrated, sterilized via heating it at temperatures above 85 °C for 40–60 min, and then spray dried [31].

2.2. Experiment models

2.2.1. in vitro model

Mouse vascular aortic smooth muscle cells (MOVAS; American Type Culture Collection, Manassas, VA, USA) were cultured in Dulbecco's Modified Eagle's Medium containing 10% fetal bovine serum and 1% penicillin/streptomycin. For establishing an in vitro MOVAS model, the cells were treated with 0.4 mL of serum from water-treated WKY, water-treated SHR, 150 mg/kg/day ECE-treated SHR for 48 hr at 37 °C in a 5% CO_2 atmosphere incubator.

2.2.2. PGC-1α shRNA transfection to the MOVAS

MOVAS were transfected into PGC-1α shRNA (Cat. SC-38885-SH, Santa cruz bioltechnology, CA, USA) using Lipofectamine 3000 reagent (Cat. L3000001, Invitrogen, CA, USA) following the manufacturer's protocols. Briefly, MOVAS were seeded in 60 mm culture dishes for 24 hr before transfection. Then, the seeded cells were treated with PGC-1α shRNA (1 μg) with lipofectamine for 10 hr. After transfection, the 0.4 mL of serum from water-treated WKY, water-treated SHR, 150 mg/kg/day ECE-treated SHR mice were applied to the cells for 48 hr at 37 °C in a 5% CO_2 atmosphere incubator.

2.2.3. PGC-1α overexpression to the MOVAS using ZLN005 (PGC-1α activator)

MOVAS were treated with ZLN005 (Cat. SML0802, Sigma-Aldrich, St. Louis, MO, USA) for PGC-1α overexpression. MOVAS were seeded in 60 mm culture dishes for 24 hr before overexpression. Then, the seeded cells were treated with ZLN005 (20 μM) for 36 hr. After overexpression, the 0.4 mL of serum from water-treated WKY, water-treated SHR, 150 mg/kg/day ECE-treated SHR mice were applied to the cells for 48 hr at 37 °C in a 5% CO_2 condition.

2.2.4. in vivo model

Male SHRs (aged 8 weeks, $n = 25$) and WKY rats (aged 8 weeks, n = 5) were obtained from Orient Bio (Seongnam, Republic of Korea) and housed at a constant temperature of ~23 °C, relative humidity of 50%, and in 12/12 hr dark/light cycle. After 1 week for acclimatization, the SHRs were randomly categorized into four groups. For 4 weeks, all rats were administered drinking water (WKY/water, SHR/water; n = 5 each) orally, and the SHRs were orally administered ECE (50 mg/kg/day, SHR/ECE50, n = 5; 100 mg/kg/day, SHR/ECE100, n = 5; 150 mg/kg/day, or SHR/ECE150, n = 5). After 4 weeks, the aortas and serum from all rats were harvested for this study. All experiments were repeated thrice per rat. All experiments were performed according to the ethical principles of the Institutional Animal Care and Use Committee of Gachon University (approval no. LCDI-2019–0121).

2.3. Sample preparation

2.3.1. RNA extraction

RNA extraction was performed according to the manufacturer's instructions. Briefly the cells were homogenized by adding 1 mL of RNAiso (Cat. 9108, Takara, Tokyo, Japan) to ice using a disposable pestle, and the homogenates were kept at room temperature for 5 min. Additionally, 0.2 mL of chloroform was added to the samples, which were mixed via vortexing and then kept at room temperature for 5 min before being centrifuged at 12,000 × g for 15 min at 4 °C, and once in the aqueous phase the samples were transferred to new tubes. The aqueous phase was mixed with 0.5 mL of isopropanol, kept for 10 min at room temperature, and centrifuged at 12,000 × g for 10 min at 4 °C. Then, the isopropanol was discarded, leaving only the RNA pellet. A 0.5 mL amount of 70% ethanol was added to the pellet, and it was centrifuged at 7000 × g for 5 min at 4 °C. Then, the supernatant was discarded, air-dried, and dissolved in 50 μL of diethyl pyrocarbonate-treated water.

2.3.2. Complementary DNA (cDNA) synthesis

cDNA synthesis (Cat. 6210 A, Takara, Tokyo, Japan) was performed according to the manufacturer's instructions. Briefly, the RNA was quantified by Nanodrop (Thermo scientific, USA). Additionally, 1 μg of RNA, 1 μL of Oligo dT Primer, 1 μL of dNTP Mixture were added to RNase Free dH_2O to make a total volume of 10 μL. The mixture was incubated for 5 min at 65 °C and cooled down on ice, and 4 μL of 5X PrimeScript Buffer, 0.5 μL of RNase Inhibitor, 1 μL of PrimeScript RTase, and 4.5 μL of RNase Free dH_2O were added to make a total volume of 20 μL. The mixture was mixed, incubated for 45 min at 42 °C and then for 5 min at 95 °C, and it was then cooled down on ice.

2.3.3. Protein isolation

The cells and skin tissue were lysed with EzRIPA buffer containing protease and phosphatase inhibitors (ATTO Corporation, Tokyo, Japan) and homogenized at 6.0 m/s for 10 cycles (running 40 s, interrupt 60 s) with a bead homogenizer (BIOPREP-24R, Allsheng Instrument Co., Ltd, Hangzhou, China). Then, the homogenized samples were sonicated and centrifuged at 14,000 × *g* for 20 min at 4 °C. Then, the supernatants were transferred to a new tube, and the protein was quantified using a bicinchoninic acid assay kit (BCA kit; Thermo Fisher Scientific, Waltham, MA, USA).

2.3.4. Paraffin-embedded tissue

The aorta tissues were fixed in cold 4% paraformaldehyde (Sigma-Aldrich, St. Louis, MO, USA) and dissolved in PBS for 24 h. After washing the fixed aortas in tap water for 30 min, it was dehydrated and wax infiltrated using a tissue processor (Tissue-Tek VIP® 5 Jr, SAKURA Finetek, Tokyo, Japan), and then the aortas were embedded using an embedding machine (Tissue-Tek® TEC™ 6, SAKURA Finetek).

2.4. Quantitative real-time polymerase chain reaction (qRT-PCR)

qRT-PCR was performed on the cDNA using the CFX384 TouchTM Real-Time PCR detection system. Briefly, 200 ng of cDNA, 5 μL of SYBR premix (Cat. RR420A, Takrara, Tokyo, Japan), 0.4 μM forward and reverse primers (Table S1) were mixed, and the threshold cycle numbers were determined using CFX ManagerTM software (Bio-rad laboratories, Hercules, CA, USA).

2.5. Enzyme-linked immunosorbent assay (ELISA)

2.5.1. Sandwich ELISA

To measure the PGC-1α–NRF2 binding in the cells and aortas, 96-well microplates were coated with anti-PGC-1α (Table S2) antibodies diluted in 100 nM carbonate and bicarbonate-mixed buffer, adjusted to pH 9.6, and incubated overnight at 4 °C. The microplates were then washed with phosphate-buffered saline (PBS) containing 0.1% Triton X-100 (TPBS). The remaining protein-binding sites were blocked using 5% skim milk for 6 hr at room temperature. After washing with PBS, 30 μg protein samples were distributed into each well and incubated overnight at 4 °C. Each well was rinsed with TPBS and then incubated with anti-NRF2 (Table S2) and diluted in PBS overnight at 4 °C. After washing, a peroxidase-conjugated secondary antibody (Table S2, Vector Laboratories, Burlingame, CA, USA) was loaded for 4 hr at room temperature. Tetramethylbenzidine solution was added, followed by incubation for 15–20 min at room temperature. The stop solution that was used 2 N sulfuric acid. Optical density was measured at a wavelength of 450 nm using a microplate reader (Spectra Max Plus; Molecular Devices, San Jose, CA, USA).

2.5.2. Indirect ELISA

To measure the compound 8-hydroxy-2′-deoxyguanosine (8-OHdG; Table S2) in the cells and aortas, 96-well microplates were coated in 100 nM carbonate and bicarbonate-mixed buffer, adjusted to pH 9.6, and incubated overnight at 4 °C. The microplates were then washed with PBS containing 0.1% Triton X-100 (TPBS). The remaining protein-binding sites were blocked using 5% skim milk for 6 hr at room temperature. After washing with PBS, 30 μg of protein samples was distributed into each well and incubated overnight at 4 °C. Each well was rinsed with TPBS and then incubated with anti-8-OHdG diluted in PBS overnight at 4 °C. After washing, a peroxidase-conjugated secondary antibody (Table S2, Vector Laboratories, Burlingame, CA, USA) was loaded for 4 h at room temperature. Tetramethylbenzidine solution was added, followed by incubation for 15–20 min at room temperature. The stop solution that was used was 2 N sulfuric acid. Optical density was measured at a wavelength of 450 nm using a microplate reader (Spectra Max Plus; Molecular Devices, San Jose, CA, USA).

NADPH oxidase activity in the aorta was determined for each group using the appropriate kit (Cat. ab65349, abcam, Cambridge, UK) according to the manufacturer's instructions. Briefly, 30 mg of aorta sample was homogenized with 0.5 mL of extraction buffer, moved to new tube, and spun for 5 min, and the supernatant was then moved into new tube. An amount of 100 μL of sample and 100 μL of background reaction mix were transferred into new wells. Then, 10 μL of NADPH developer was added to the samples and incubated for 1 hr. Absorbance was detected at 450 nm on a microplate reader.

Calcium quantification was performed using a commercial kit (Cat. ab102505, abcam, Cambridge, UK). Briefly, 10 mg of aorta sample was washed in PBS, 500 μL of calcium assay buffer was added, the tissue was homogenized with a homogenizer, centrifuged for 5 min, and moved to a new tube. An amount of 10 μL was transferred into new wells. Then, 90 μL of chromogenic reagent and 60 μL of calcium assay buffer were added into each well and incubated for 5 min. Absorbance was detected at 575 nm on a microplate reader.

2.6. Western blotting

A total of 30 μg of the isolated proteins was separated on 8–12% polyacrylamide gels and transferred to polyvinylidene fluoride membranes (Millipore, Burlington, MA, USA) using a power station (ATTO, Osaka, Japan). The membranes were blocked using 5% skim milk and washed with Tris-buffered saline with 0.1% Tween 20 (TTBS), and the membranes were incubated with primary antibodies (Table S2) for 12 h at 4 °C. After, the membranes were washed with TTBS and then incubated with a peroxidase-conjugated secondary antibody (Table S2, Vector Laboratories, Burlingame, CA, USA) and washed with TTBS. Then, a chemiluminescence detection reagent (GE Healthcare, Chicago, IL, USA) was used on the membranes to visualize the immunoreactive proteins.

2.7. Immunohistochemistry (3,3-diaminobenzidine [DAB])

The aorta tissue blocks were cut into sections that were 7 μm thick, placed on coated slides, and dried for 24 hr at 45 °C. The slides were deparaffinized and incubated in normal animal serum to block antibody-nonspecific binding were and then incubated with primary antibodies (Table S2) at 4 °C overnight and were rinsed thrice with PBS. The slides were then treated with biotinylated secondary antibodies (Table S2, Vector Laboratories, Burlingame, CA, USA) for 1 hr at room temperature and were then rinsed thrice with PBS. Then, the slides were incubated with an ABC reagent (Vector Laboratories, Burlingame, CA, USA) for 30 min and rinsed thrice with PBS. Next, the slides were left to react with DAB substrate for up to 2–5 min and were then mounted on a cover slip and distyrene–plasticizer–xylene mounting solution (Sigma-Aldrich, St. Louis, MO, USA). Images were obtained using a light microscope (Olympus, Tokyo, Japan), and the intensity of the brown color that was visible on the slides was quantified using Image J software (NIH, Bethesda, MD, USA) [32].

2.8. Determination of mitochondrial ROS

A MitoSOX™ Red fluorescent probe (Cat. M36008, Molecular Probes, Inc., Eugene, OR, USA) was used to visualize mitochondrial superoxide production according to the manufacturer's protocols. Briefly, MOVAS grown on glass that was 12 mm thick were washed twice with PBS and incubated with 2.5 μM MitoSOX-Red reagent in the dark at 37 °C. Cells were washed gently three times with warm PBS. To confirm the mitochondrial localization of MitoSOX-Red, the cells were loaded with 300 nM MitoTracker-Green (Cat. M7514, Molecular Probes, Inc., Eugene, OR, USA) for 30 min and imaged immediately after using fluorescence microscopy (LSM-700) at Core-facility for Cell to In-vivo imaging (Incheon, Korea). The mean fluorescence intensities of MitoSOX-Red and MitoTracker-Green were divided by the number of cells in each image and quantified using Image J software.

2.9. Damaged mitochondrial DNA assay

Mitochondrial DNA damage was assessed using a mouse DNA Damage Analysis Kit (Cat. DD2M, Detroit R&D, Detroit MI, USA) according to manufacturer's instructions. Briefly, the aortas and cells were lysed in lysis buffer (5 M sodium chloride, 1 M tris, 0.5 M EDTA, 10% SDS and 0.3 mg/mL proteinase K) at 56 °C for 24 hr and then inactivated to proteinase K at 95 °C for 10 mins. The lysates were diluted in nuclease-free water. Samples (5 ng/μL DNA) were subjected to PCR reaction, after which the 10X diluted PCR reaction product was subjected to real-time PCR. The final concentrations of the damaged mitochondrial DNA were calculated from the 8.2 kb standard curve plotted using the 8.2 kb real-time standard supplied with the kit.

2.10. Mitochondrial DNA copy number assay

Mitochondrial DNA copy number was assessed by qRT-PCR using a mouse mitochondrial DNA Copy Number Assay Kit (Cat. MCN3, Detroit R&D, Detroit MI, USA) according to manufacturer's instructions.

2.11. Alizarin red S staining

To validate the amount of calcium in the aorta tissue, Alizarine Red S staining was conducted. The deparaffinized slides were washed twice with distilled water and then incubated with 0.2% Alizarine Red S, incubated for 5 min, and dehydrated in acetone. The stained slides were stained with hematoxylin for nuclei counting, cleared with xylene, and mounted using DPX mounting medium (Sigma-Aldrich).

2.12. Statistical analysis

Statistical significance was determined via the Kruskal–Wallis test for comparisons between each group followed by a post hoc Mann-Whitney U test. All the results are presented as the means ± standard deviations, and all statistical analyses were performed by using SPSS version 22 (IBM Corporation; Armonk, NY, USA).

3. Results

3.1. ECE increases PGC-1α–NRF2 binding, SIRT3 expression, and SOD2 activity in the MOVAS and the aortas of SHRs

First, we evaluated whether ECE increased the expression of SIRT3 and SOD2 activity via PGC-1α. MOVAS were treated with serums obtained from WKY/water, SHR/water, and SHR/ECE (150 mg/kg) animals. The mRNA expression of PGC-1α in the SHR/water serum-treated MOVAS was lower than that found in the WKY/water serum-treated MOVAS. However, the mRNA expression of PGC-1α was significantly increased by treating serum from the SHR/ECE group compared to in the MOVAS treated with serum from the SHR/water group. In the PGC-1α silencing MOVAS, PGC-1α expression was not changed by the treating serum from either the SHR/water or SHR/ECE groups compared to the treating serum from the WKY/water group (Fig. 1A). Upon overexpression of PGC-1α by ZLN005, mRNA expression of PGC-1α in all three MOVAS groups was increased. mRNA expression of PGC-1α was increased in response to ZLN005, even after administration of SHR/water serum (Fig. S1A).

The mRNA expression of NRF2 in the SHR/water serum-treated MOVAS was lower than that found in the WKY/water se-rum-treated MOVAS. However, the mRNA expression of NRF2 was significantly increased by treating serum from the SHR/ECE group compared to in the MOVAS treated with serum from the SHR/water group. The decreasing expression of NRF2 which induced by treating SHR/water serum to MOVAS was disappeared when PGC-1α overexpression was induced by ZLN005 (Fig. S1B).

The PGC-1α–NRF2 binding ratio evaluated with sandwich ELISA in the SHR/water serum-treated MOVAS was significantly lower than the MOVAS that treated with the serum from the WKY/water group. It was significantly increased by the serum from the SHR/ECE group compared to MOVAS that treated with the serum from the SHR/water group. However, the PGC-1α–NRF2 binding ratio in the PGC-1α silencing MOVAS was not decreased by the treating serum from the SHR/water group compared to that from the WKY/water group. The PGC-1α–NRF2 binding ratio in the PGC-1α silencing MOVAS was not increased by treating serum from the SHR/ECE group compared to that from the SHR/water group (Fig. 1B).

The SIRT3 expression evaluated by western blotting in the MOVAS-treated serum from the SHR/water group was significantly lower than the MOVAS that treated with serum from the WKY/water group. SIRT3 expression was significantly increased by the treating serum from the SHR/ECE group compared to the MOVAS that treated with the serum from the SHR/water group. Those changes were disappeared by PGC-1α silencing (Fig. 1C and S1C). Upon overexpression of PGC-1α by ZLN005, mRNA expression of SIRT3 in all three MOVAS groups was increased. mRNA expression of SIRT3 was increased in response to ZLN005, even after administration of SHR/water serum (Fig. S1D).

The ratio of acetylated SOD2 (Ac-SOD2) and SOD2 was higher in the serum from the SHR/water-treated MOVAS than it was in the serum from the WKY/water-treated MOVAS. It was decreased by the treating serum from SHR/ECE group compared to the MOVAS treating serum from the SHR/water group. Since SOD2 activity is increased by deacetylation, the fact that Ac-SOD2/SOD2 was decreased by ECE suggested that SOD2 activity was increased by ECE. These changes were eliminated by PGC-1α silencing (Fig. 1C and S1E).

PGC-1α expression was significantly lower in the aortas from the SHRs than it was in the aortas of the WKY rats but increased after the administration of 100 and 150 mg/kg of ECE (Fig. 1D and S1F). The increasing effect was the highest at 150 mg/kg of ECE.

The PGC-1α–NRF2 binding ratio was significantly lower in the aortas of SHRs than it was in the aortas of the WKY rats, but it increased dose-dependently after ECE treatment (Fig. 1E).

We evaluated the expression of SIRT3 and Ac-SOD2 by staining since we only wanted to evaluate their expression in the smooth muscle cells of the aortic medial layer separately from their expression in the intima (Fig. 1F). The SIRT3 expression in the medial layer of the aorta was significantly lower in SHRs than it was in the WKY rats but increased after ECE treatment. The most prominent increase effect was shown with 150 mg/kg of ECE (Fig. 1F and S1G). The Ac-SOD2 expression in the medial layer of the aorta was significantly higher in the SHRs than it was in the WKY rats but decreased dose-dependently after ECE treatment (Fig. 1F and S1H).

3.2. ECE decreases mtDNA damage and mtROS generation

Mitochondrial superoxide (MitoSOX) Red, as a novel fluorescent dye, selectively detects superoxide in the mitochondria of living cells [33].

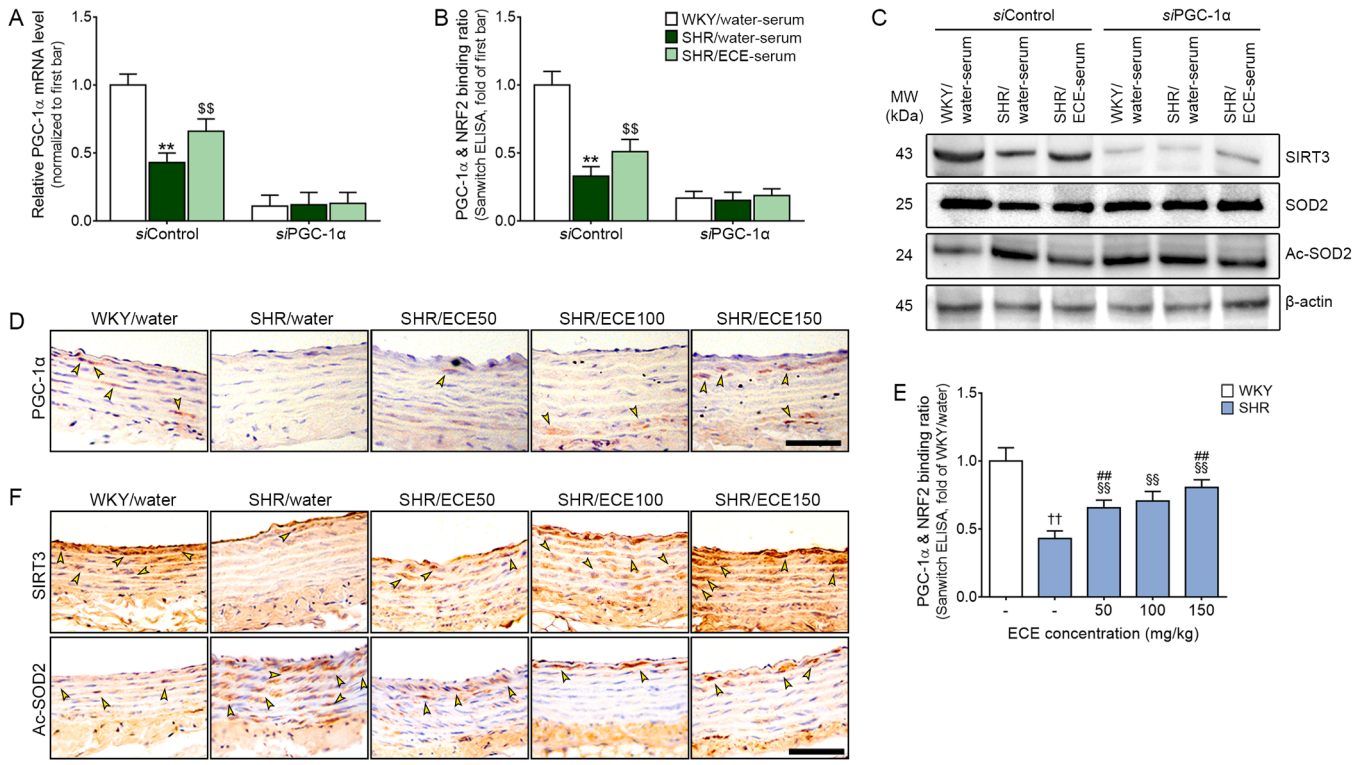

Fig. 1. Regulation of PGC-1α, NRF2, and SIRT3 expression and SOD2 hyperacetylation by ECE treatment. (A-C) After PGC-1α silencing in the MOVAS (or not), PGC-1α mRNA expression was analyzed via real time PCR (A). The PGC-1α–NRF2 binding ratio in the MOVAS was analyzed by sandwich ELISA (B). SIRT3, SOD2, and Ac-SOD2 expression in the MOVAS were analyzed by western blotting (C). (D) The PGC-1α expression in the aortas of WKY, SHR, and SHR/ECEs was analyzed by immunohistochemistry (scale bar = 100 μm). The yellow arrows represent positive signals. (E) PGC-1α–NRF2 binding ratio in the animal aortas was determined by sandwich ELISA. (F) SIRT3 and Ac-SOD2 expression in the aortas of the WKY, SHR, and SHR/ECEs groups were analyzed in the aorta by immunohistochemistry (scale bar = 100 μm). The yellow arrows represent positive signals. Data are presented as mean±standard deviation. * *, $p < 0.01$ SHR/water-serum vs. WKY/water-serum; $$, $p < 0.01$ SHR/ECE-serum vs. SHR/water-serum; ††, $p < 0.01$ SHR/water vs. WKY/water; §§, $p < 0.01$ SHR/ECEs vs. SHR/water; ##, $p < 0.01$ SHR/ECEs vs. SHR/ECE100 (Mann–Whitney U test). Ac, acetyl; ECE, *Ecklonia cava* extract; ECE-serum, Serum from *Ecklonia cava* extract treated rat; ELISA, enzyme-linked immunosorbent assay; NRF2, nuclear factor erythroid 2-related factor 2; PGC-1α, peroxisome proliferator-activated receptor gamma coactivator-1 alpha; SIRT3, sirtuin 3; SHR, spontaneous hypertensive rat; si, silencing; SOD2, superoxide dismutase 2; water-serum, Serum from water treated rat; WKY, Wistar Kyoto.

To evaluate ECE's effect on decreasing mtROS generation, we performed MitoSOX Red staining in the MOVAS-treating animal serums. To evaluate the ROS in the mitochondria, we performed MitoSOX Red co-staining with mitotracker, which is a mitochondria marker. The intensity of the co-stained MitoSOX Red and mitotracker was higher in the SHR/water serum-treated MOVAS than it was in the WKY/water serum-treated MOVAS. It was significantly lower in the SHR/ECE serum-treated MOVAS than it was in the SHR/water serum-treated MOVAS. These changes were eliminated by PGC-1α silencing (Fig. 2A and 2B).

The 8-Hydroxy-2′-deoxyguanosine (8-OHdG) is frequently used as an indicator of mtDNA damage [34]. It was significantly higher in the SHR/water serum-treated MOVAS than it was in the WKY/water serum-treated MOVAS. It was decreased in the SHR/ECE serum-treated MOVAS than it was in the SHR/water serum-treated MOVAS. These changes were eliminated by PGC-1α silencing (Fig. 2C).

Damaged mtDNA were also evaluated using the mitochondrial DNA damage assay. The amount of damaged mtDNA was significantly higher in the SHR/water serum-treated MOVAS than it was in the WKY/water serum-treated MOVAS. It was lower in the SHR/ECE serum-treated MOVAS than it was in the SHR/water serum-treated MOVAS. These changes were eliminated by PGC-1α silencing (Fig. 2D).

The expression of 8-OHdG in the medial layer of the aortas of the SHRs was significantly higher than it was in the aortas of the WKYs. It was decreased dose-dependently by ECE (Figs. 2E and 2F).

The amount of damaged mtDNA in the medial layer of the aortas of the SHRs was significantly higher than that observed in the aortas of the WKYs. It was decreased dose-dependently by ECE (Fig. 2G).

3.3. ECE modulates mitochondrial function

DRP1 and fission 1 (FIS1) expression (mitochondrial fission markers) in the SHR/water serum-treated MOVAS was significantly higher than they were in the WKY/water serum-treated MOVAS. Their expression was lower in the SHR/ECE serum-treated MOVAS than they were in the SHR/water serum-treated MOVAS. However, these changes were eliminated by PGC-1α silencing (Fig. 3A, S2A, and S2B). Upon overexpression of PGC-1α by ZLN005, mRNA expression of FIS and DRP1 in all three MOVAS groups was decreased. mRNA expression of FIS and DRP1 was decreased in response to ZLN005, even after administration of SHR/water serum (Fig. S2C and S2D).

Mitofusin 2 (MFN2) and OPA1 expression (mitochondrial fusion markers) in the SHR/water serum-treated MOVAS were significantly lower than they were in the WKY/water serum-treated MOVAS. Their expression was higher in the SHR/ECE serum-treated MOVAS than they were in the SHR/water serum-treated MOVAS. However, these changes were eliminated by PGC-1α silencing (Fig. 3A, S2E, and S2F). Moreover, MFN2 and OPA1 expression was not decreased by treating serum from SHR/water compared to MOVAS treated with WKY/water, when PGC-1α overexpression was induced by ZLN005 (Fig. S2G and S2H).

BCL2 Interacting Protein 3 (BNIP3) and autophagy related 12 (ATG12) expression were evaluated as mitophagy markers [35,36]. BNIP3 and ATG12 expression in the SHR/water serum-treated MOVAS were significantly lower than they were in the WKY/water

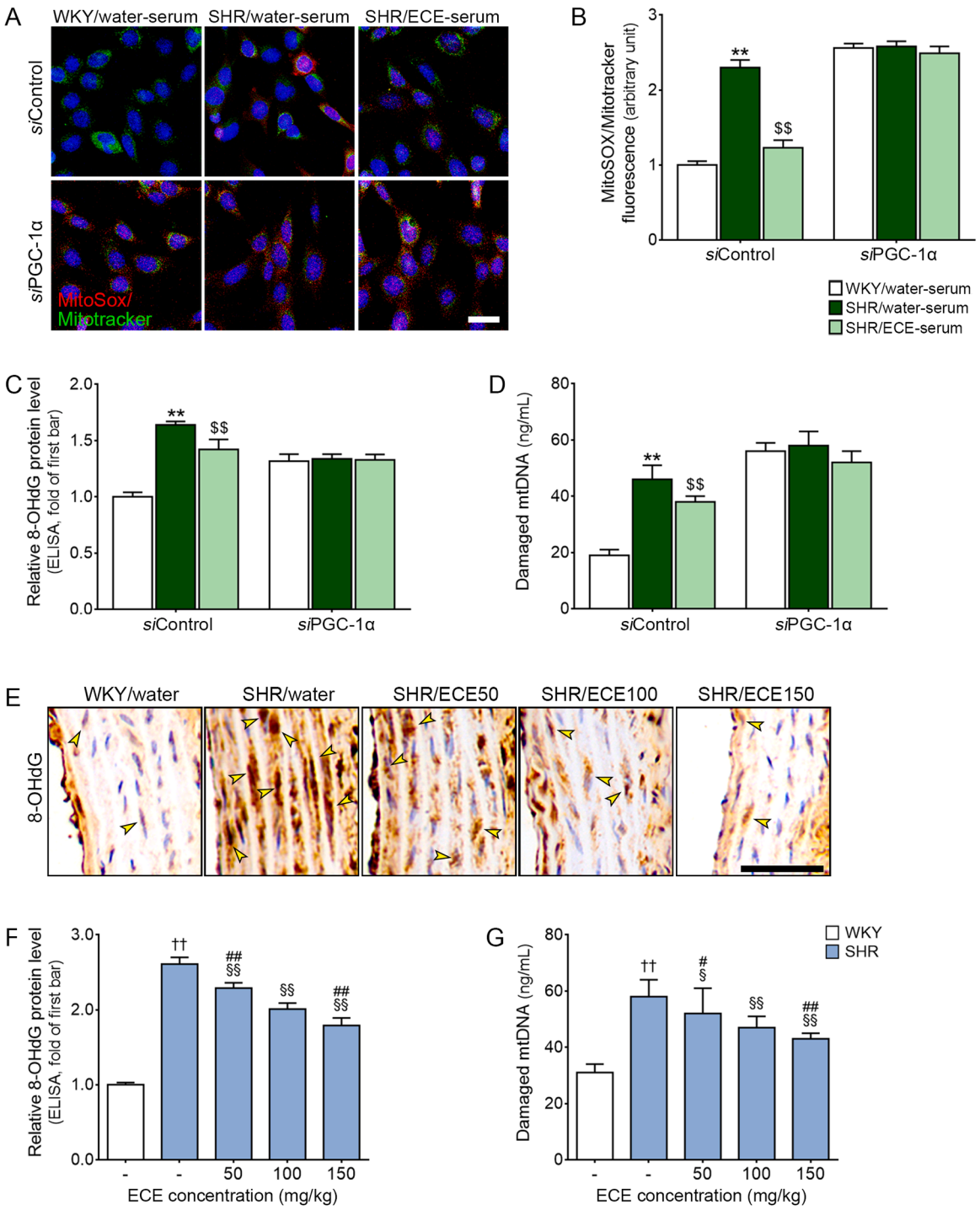

Fig. 2. Regulation of mtROS and mtDNA expressions by ECE treatment. (A and B) After PGC-1α silencing in the MOVAS (or not), MitoSOX Red expression with mitotracker was analyzed by fluorescence microscopy (scale bar = 50 μm; A). The intensity of MitoSOX Red staining increased in the SHR/water serum-treated MOVAS and decreased in the SHR/ECE serum-treated MOVAS (B). (C) The expression of 8-OHdG in the MOVAS was analyzed by indirect ELISA. After PGC-1α silencing in the MOVAS (or not), the expression of 8-OHdG increased in the SHR/water serum-treated MOVAS and decreased in the SHR/ECE serum-treated MOVAS. (D) The damaged mtDNA in the MOVAS was analyzed by qRT-PCR. After PGC-1α silencing in the MOVAS (or not),the damaged mtDNA increased in the SHR/water serum-treated MOVAS and decreased in the SHR/ECE serum-treated MOVAS. (E and F) The expression of 8-OHdG in the aortas of WKY, SHR, and SHR/ECEs was determined by immunohistochemistry. The yellow arrows represent positive signals (scale bar = 100 μm; A) and indirect ELISA (B). The expression of 8-OHdG increased in the SHR/water group and decreased after ECE treatment. (G) The damaged mtDNA in the aortas of WKY, SHR, and SHR/ECEs was analyzed by qRT-PCR. The damaged mtDNA increased in the SHR/water group and decreased after ECE treatment. Data are presented as mean ± standard deviation. * *, $p < 0.01$ SHR/water-serum vs. WKY/water-serum; $$, $p < 0.01$ SHR/ECE-serum vs. SHR/water-serum; ††, $p < 0.01$ SHR/water vs. WKY/water; §§, $p < 0.01$ SHR/ECEs vs. SHR/water; ##, $p < 0.01$ SHR/ECEs vs. SHR/ECE100 (Mann–Whitney U test). 8-OHdG, 8-hydroxy-2′-deoxyguanosine; ECE, *Ecklonia cava* extract; ECE-serum, Serum from *Ecklonia cava* extract treated rat; ELISA, enzyme-linked immunosorbent assay; MitoSOX, mitochondrial superoxide; mtDNA, mitochondrial deoxyribonucleic acid; PGC-1α, peroxisome proliferator-activated receptor gamma coactivator-1 alpha; qRT-PCR, Quantitative real-time polymerase chain reaction; SHR, spontaneous hypertensive rat; si, silencing; water-serum, Serum from water treated rat; WKY, Wistar Kyoto.

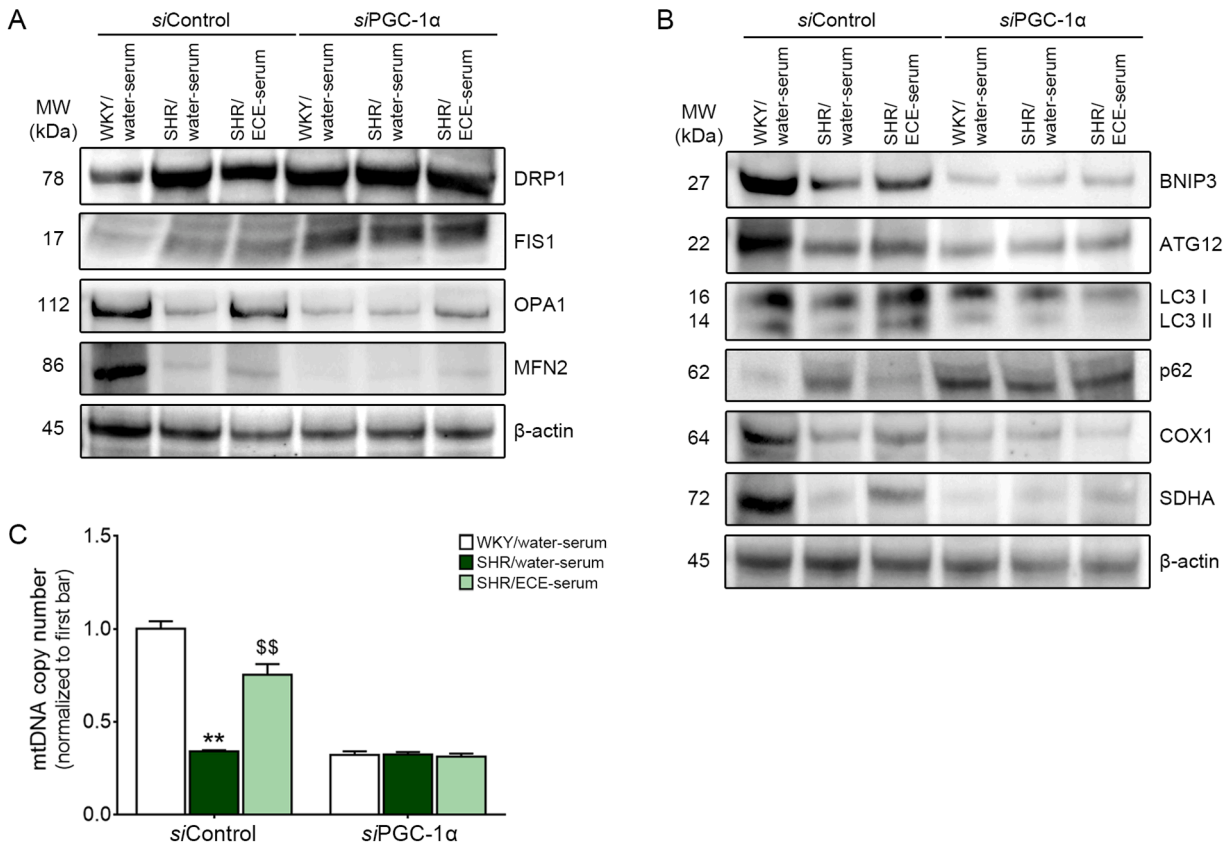

Fig. 3. Regulation of mitochondrial function by ECE treatment in the MOVAS. (A) After PGC-1α silencing in the MOVAS (or not), the DRP1, FIS1, OPA1 and MFN2 expression in the MOVAS were analyzed by western blotting. DRP1 and FIS1 were used as the mitochondrial fission marker. OPA1 and MFN2 were used as the mitochondrial fusion marker. (B) BNIP3, ATG12, LC3, COX1, p62, and SDHA expression in the MOVAS was analyzed by western blotting. BNIP3, ATG12, LC3, and p62 were used as mitophagy markers. COX1 and SDHA were used as mitochondrial biogenesis markers. (C) mtDNA copy number quantification were validated by qRT-PCR using genomic DNA. Data are presented as mean ± standard deviation. * *, $p < 0.01$ SHR/water-serum vs. WKY/water-serum; $$, $p < 0.01$ SHR/ECE-serum vs. SHR/water-serum (Mann–Whitney U test). ATG12, autophagy-related 12; BNIP3, BCL2 interacting protein 3; COX1, cytochrome c oxidase 1, DRP1, dynamin-related protein 1; ECE, *Ecklonia cava* extract; ECE-serum, Serum from *Ecklonia cava* extract treated rat; LC3, Microtubule-associated protein 1 A/1B-light chain 3; MFN2, mitofusin 2; mtDNA, mitochondrial deoxyribonucleic acid; OPA1, optic atrophy protein 1; PGC-1α, peroxisome proliferator-activated receptor gamma coactivator-1 alpha; qRT-PCR, real-time quantitative reverse transcription polymerase chain reaction; SDHA, succinate dehydrogenase complex flavoprotein subunit A; SHR, spontaneous hypertensive rat; si, silencing; water-serum, Serum from water treated rat; WKY, Wistar Kyoto.

serum-treated MOVAS. Their expressions were higher in the SHR/ECE serum-treated MOVAS than they were in the SHR/water serum-treated MOVAS. However, these changes were eliminated by PGC-1α silencing (Fig. 3B, S2I, and S2J). Moreover, BNIP3 and ATG12 expression was not decreased by treating serum from SHR/water compared to WKY/water, when PGC-1α overexpression was induced by ZLN005 (Fig. S2K and S2L).

Microtubule-associated proteins 1 A/1B light chain 3 (LC3) and p62 is involve in mitophagy process by forming autophagosome component [37,38]. The expression ratio of LC3II/LC3I in the SHR/water serum-treated MOVAS were significantly lower than it was in the WKY/water serum-treated MOVAS. The expression ratio of LC3II/LC3I was higher in the SHR/ECE serum-treated MOVAS than it was in the SHR/water serum-treated MOVAS. However, the increasement was eliminated by PGC-1α silencing (Fig. 3B and S2M). Moreover, LC3 mRNA expression was not increased by treating serum from SHR/ECE compared to SHR/water, when PGC-1α overexpression was induced by ZLN005 (Fig. S2O). P62 expression in the SHR/water serum-treated MOVAS was significantly higher than it was in the WKY/water serum-treated MOVAS. Their expression was lower in the SHR/ECE serum-treated MOVAS than it was in the SHR/water serum-treated MOVAS. However, the decrement was eliminated by PGC-1α silencing (Fig. 3B and S2N). Upon overexpression of PGC-1α by ZLN005, mRNA expression of FIS and DRP1 in all three MOVAS groups was decreased. mRNA expression of P62 was decreased in response to ZLN005, even after administration of SHR/water serum (Fig. S2C and S2P).

Cytochrome c oxidase (COX)1 and succinate dehydrogenase complex flavoprotein subunit A (SDHA), mitochondrial biogenesis markers [39], were determined. The COX1 and SDHA expression in the SHR/water serum treated MOVAS were significantly lower than they were in the WKY/water serum-treated MOVAS. Their expression was higher in the SHR/ECE serum-treated MOVAS than they were in the SHR/water serum-treated MOVAS. However, these changes were eliminated by PGC-1α silencing (Fig. 3B, S2Q, and S2R). Moreover, COX1 and SDHA expression was not decreased by treating serum from SHR/water compared to WKY/water, when PGC-1α overexpression was induced by ZLN005 (Fig. S2S and S2T).

The mtDNA copy number which is also a well-known marker of mitochondrial biogenesis was determined [40]. The mtDNA copy number in the SHR/water serum treated MOVAS were significantly lower than they were in the WKY/water serum-treated MOVAS. The mtDNA copy number was higher in the SHR/ECE serum-treated MOVAS than it was in the SHR/water serum-treated MOVAS. However, these changes were eliminated by PGC-1α silencing (Fig. 3C). Moreover, mtDNA copy number was not decreased by treating serum from SHR/water compared to WKY/water, when PGC-1α overexpression was induced by ZLN005 (Fig. S2U).

The DRP1 and FIS1 expressions in medial layer of the aortas in SHRs

were significantly higher than they were in the WKY rats but significantly decreased dose-dependently after ECE treatment (Fig. 4A, S3A, and S3B).

MFN2 and OPA1 expressions were significantly lower in the aortic medial layer of the SHRs than they were in the WKY rats but dose-dependently increased after ECE treatment (Fig. 4B, S3C, and S3D).

BNIP3 expression were significantly lower in the aortic medial layer of the SHRs than they were in the WKY rats but increased dose-dependently after ECE treatment. ATG12 expression was significantly lower in the aortic medial layer of the SHRs than they were in the WKY rats but was increased by ECE. There was no significant difference between 100 mg/kg ECE and 150 mg/kg ECE (Fig. 4C, S3E, and S3F).

COX1 and SDHA expressions were significantly lower in the aortic medial layer of the SHRs than they were in the WKY rats and increased dose-dependently after ECE treatment (Fig. 4D, S3G, and S3H).

3.4. ECE decreases NADPH oxidase activity, the PI3K/AKT pathway, and NF-κB

The NADPH oxidase activity in the aortas of the SHRs was

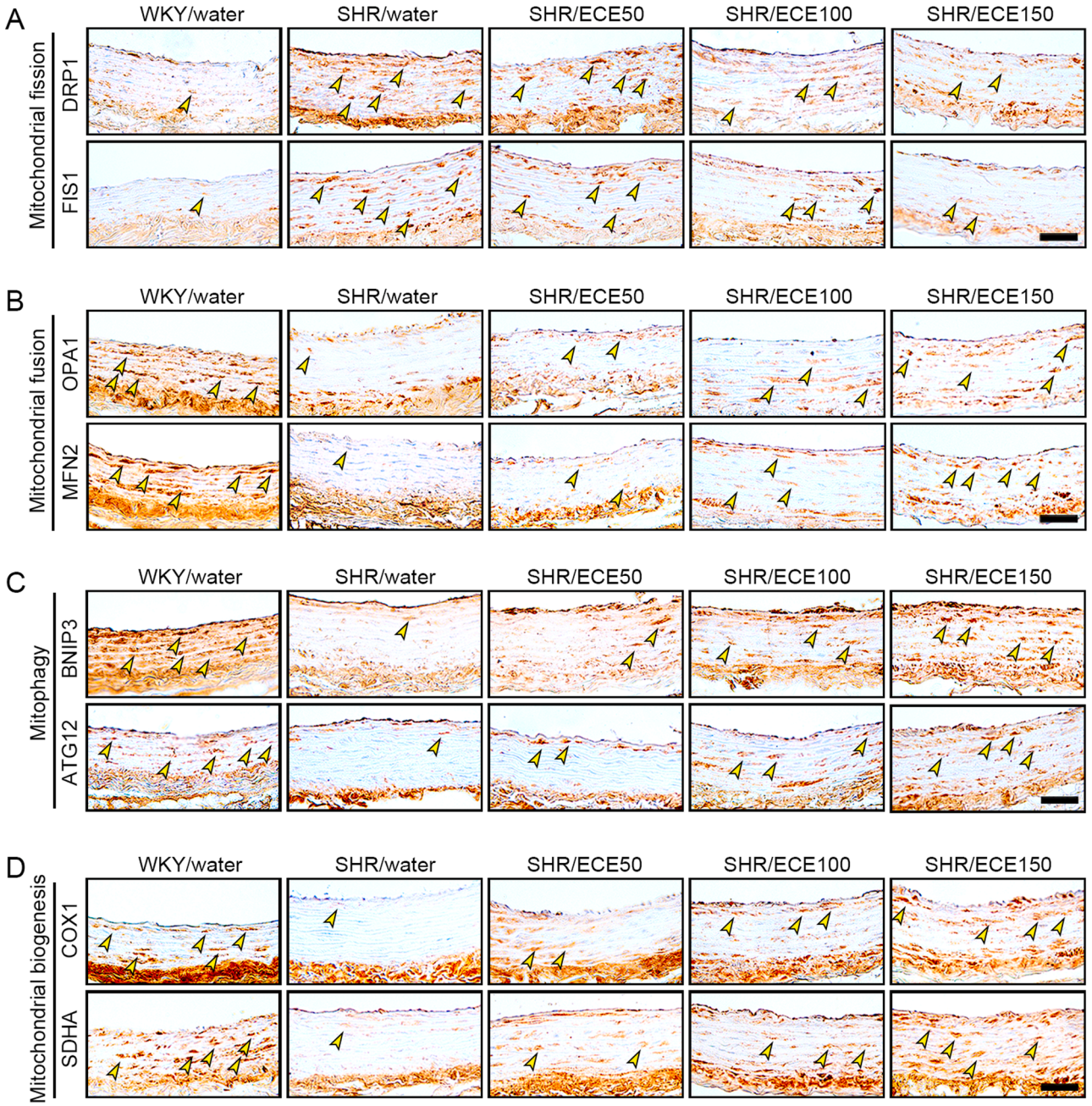

Fig. 4. Regulation of mitochondrial function by ECE treatment in the rat. (A) DRP1 and FIS1 expression in the aortas of WKY, SHR, and SHR/ECEs were analyzed by immunohistochemistry. (B) OPA1 and MFN2 expression in the aortas of WKY, SHR, and SHR/ECEs were analyzed by immunohistochemistry. (C) BNIP3 and ATG12 expression in the aortas of WKY, SHR, and SHR/ECEs were analyzed by immunohistochemistry. (D) COX1 and SDHA expression in the aortas of WKY, SHR, and SHR/ECEs was analyzed by immunohistochemistry. The yellow arrows represent positive signals (scale bar = 100 μm). ATG12, autophagy-related 12; BNIP3, BCL2 interacting protein 3; COX1, cytochrome c oxidase 1, DRP1, dynamin-related protein 1; ECE, *Ecklonia cava* extract; ECE-serum, Serum from *Ecklonia cava* extract treated rat; LC3, Microtubule-associated protein 1 A/1B-light chain 3; MFN2, mitofusin 2; OPA1, optic atrophy protein 1; PGC-1α, peroxisome proliferator-activated receptor gamma coactivator-1 alpha; qRT-PCR, real-time quantitative reverse transcription polymerase chain reaction; SDHA, succinate dehydrogenase complex flavoprotein subunit A; SHR, spontaneous hypertensive rat; water-serum, Serum from water treated rat; WKY, Wistar Kyoto.

significantly higher than it was in the WKY rats but decreased significantly after ECE treatment (Fig. 5A). The decreasing effect at the ECE concentrations of 100 and 150 mg/kg of ECE was not significantly different.

The pAKT/AKT expression ratio was significantly higher in the aortas of the SHRs than it was in the WKY rats but showed a significant dose-dependent decrease after ECE treatment (Figs. 5B and 5E).

The PI3K expression was significantly higher in the aortas of the SHRs than it was in the WKY rats but showed a significant dose-dependent decrease after ECE treatment (Fig. 5C and 5E).

The number of cell nuclei that were positively stained by NF-κB in the SHRs was significantly higher than it was in the WKY rats but showed a significant dose-dependent decrease after ECE treatment (Figs. 5D and 5E).

3.5. ECE decreases osteoblast-like VSMC changes and medial calcification

RUNX2 and osteocalcin (OCN) are typical osteoblast genes [41,42]. The RUNX2 and OCN expression in the aortas of the SHRs was significantly higher than it was in the WKY rats but showed a significant dose-dependent decrease after ECE treatment (Fig. 6A and S4).

Alizarin Red S staining showed that there were more calcium-containing cells in the aorta in SHRs than in there were WKY rats, but this showed a dose-dependent decrease after ECE treatment (Figs. 6B and 6C).

The amount of calcium, which was evaluated using a calcium assay kit, was significantly higher in the aortas of the SHRs but decreased dose-dependently after ECE treatment (Fig. 6D).

4. Discussion

Excessive mtROS generation promotes mitochondrial dysfunction, impaired mitochondrial ATP generation, increased VSMC apoptosis, and VC in aged mice [43]. In hypertension, angiotensin II leads to increased mtROS generation by decreasing SIRT3/SOD2 activity [44]. Furthermore, excessive ROS generation is also involved in development of VC. Excessive ROS generation caused by H_2O_2 treatment leads to increased NADPH oxidase activity and increased RUNX2 expression via the upregulation of the PI3K/AKT pathway [45,46]. Increased oxidative stress or mtROS generation leads to increased NF-κB activity, which sequentially increases RUNX2 expression [47].

SHRs are frequently used as a primary or essential hypertension animal model [48]. SHRs are useful in studies focusing hypertension-related stroke, vascular disease, renal dysfunction, and the genetics of primary hypertension [48]. It is well known that SHRs show higher levels of oxidative stress and angiotensin II than WKY rats [49,50]. Thus, we thought that SHRs would be a good animal model that could be used to evaluate whether ECE could decrease hypertension-related VC.

ECE contains various phlorotannins, such as dieckol [31]. Dieckol is known to decrease adipogenesis by increasing AMPK activation, resulting in the possible upregulation of SIRT1 or PGC-1α [31,51]. Thus, we evaluated whether ECE decreased VC by the upregulation of PGC-1α/NFR2/SIRT3 and by increasing SOD2 activity to eventually decrease the mitochondrial dysfunction observed in hypertension. The serum obtained from WKY, SHRs, and ECE-treated SHRs were administered to MOVAS. This experiment showed that PGC-1α expression was decreased by SHR serum, and it was increased by serum from ECE-treated SHR. The PGC-1α expression in the aortic medial layer of SHRs was significantly lower than it was in the WKY rats, and it increased with ECE treatment.

Next, we analyzed PGC-1α–NRF2 binding to evaluate the effects of ECE on increasing SIRT3 activity. PGC-1α–NRF2 binding was lower in the SHR serum-treated MOVAS; however, it was increased by the SHR/ECE-serum treated MOVAS. Upon PGC-1α silencing, treatment with SHR serum was unable to decrease PGC-1α–NRF2 binding, and SHR/ECE serum could not increase PGC-1α–NRF2 binding. SIRT3 expression was decreased by the treating SHR serum, and it was increased when the SHR/ECE serum was used to treat MOVAS. Upon PGC-1α silencing, those changes were eliminated. Moreover, SHR serum could not decreased expression of SIRT3 when overexpression of PGC-1α was induced by ZNL005. This suggests that PGC-1α is involved in increasing SIRT3 expression. Ac-SOD2/SOD2, which is reversely associated with SOD2 activity, was increased by the SHR serum, and it was decreased by the SHR/ECE serum. This suggests that ECE upregulated SOD2 activity. ECE's ability to upregulate SOD2 activity was eliminated by PGC-1α silencing. This suggests that was PGC-1α involved in increased SOD2 activity by increasing the deacetylation of SOD2 via SIRT3.

PGC-1α–NRF2 binding decreased more in the SHRs than it did in the WKY rats and was restored after ECE treatment. SIRT3 expression in the aortic medial layer of the SHRs was lower than it was in the WKY rats, but it increased after ECE treatment. Ac-SOD2 expression increased in the SHRs but decreased after ECE treatment. These changes were dose dependent.

SOD2 is a key factor in decreasing mtROS generation [52]. The mtROS, which was evaluated by the MitoSOX that was co-stained with mitotracker in the SHR serum-treated MOVAS, was increased, and it was decreased by ECE. The mtDNA damage was evaluated by conducting an ELISA to determine the amount of 8-OHdG present and via an mtDNA assay. Damaged mtDNA was increased by the SHR serum treating, and it was increased by serum from ECE treated SHR. However, Neither the mtROS nor the damaged mtDNA were decreased by ECE upon PGC-1α silencing. These results suggest that PGC-1α that is upregulated by ECE leads to decreased mtROS formation and mtDNA damage.

We analyzed 8-OHdG expression in the aortas of SHRs via staining and evaluated mtDNA damage using the mtDNA damage assay. The expression of 8-OHdG in the aortic medial layer of the SHRs was higher than it was in the WKY rats but decreased after ECE treatment. The amount of damaged mtDNA in the aortas of the SHRs higher than it was in the WKY rats, and it was decreased by ECE.

Mitochondria, which are dynamic organelles, constantly renew functional organelles and fix dysfunctional and damaged ones by fission, fusion, and mitophagy [53].

Excessive ROS generation induces changes in mitochondrial dynamics [54]. Mitochondrial fission is a division process through a mitochondrion separates into two separate mitochondria, and this process is crucial for cell division [55–57]. Moreover, mitochondrial fission is necessary for the removal of damaged mitochondria via mitophagy [54–57].

Mitochondrial fusion is the process of tethering two mitochondria that allows for the renewal of damaged mtDNA and that enables intracellular energy distribution [58,59]. During mitochondrial fission, DRP1 is translocated to the outer mitochondrial membrane (OMM) from the cytosol, where it binds to other OMM proteins, such as FIS1 [54–57].

Mitochondrial fusion is mediated by OMM fusion guanosine triphosphate (GTPase) proteins, such as MFN1 and MFN2 [58,59]. After OMM fusion, the inner mitochondrial membrane (IMM) fusion GTPase proteins, such as OPA1, fuse the IMMs and share mitochondrial matrix material, thereby forming a single elongated mitochondrion [60,61].

OPA1 is also involved in mitophagy through the AMPK/OPA1 pathway [62,63]. Mitophagy is kind of autophagy that takes place in mitochondria for the purposes of the selective removal of damaged mitochondria. Mitophagy plays an essential role in the protection of mitochondrial homeostasis against excessive ROS generation and mtDNA damage [64,65]. In lactate-induced calcified VSMCs, mitochondrial dysfunction is accompanied by downregulated mitophagy [66]. During VSMC calcification, lactate induced decreased LC3II expression and BNIP3 which suggested abnormality in mitophagy [66]. However, increased mitophagy that is mediated by BNIP3 leads to decreased mitochondrial dysfunction and reduced the VSMC phenotype changes into an osteoblastic phenotype [66].

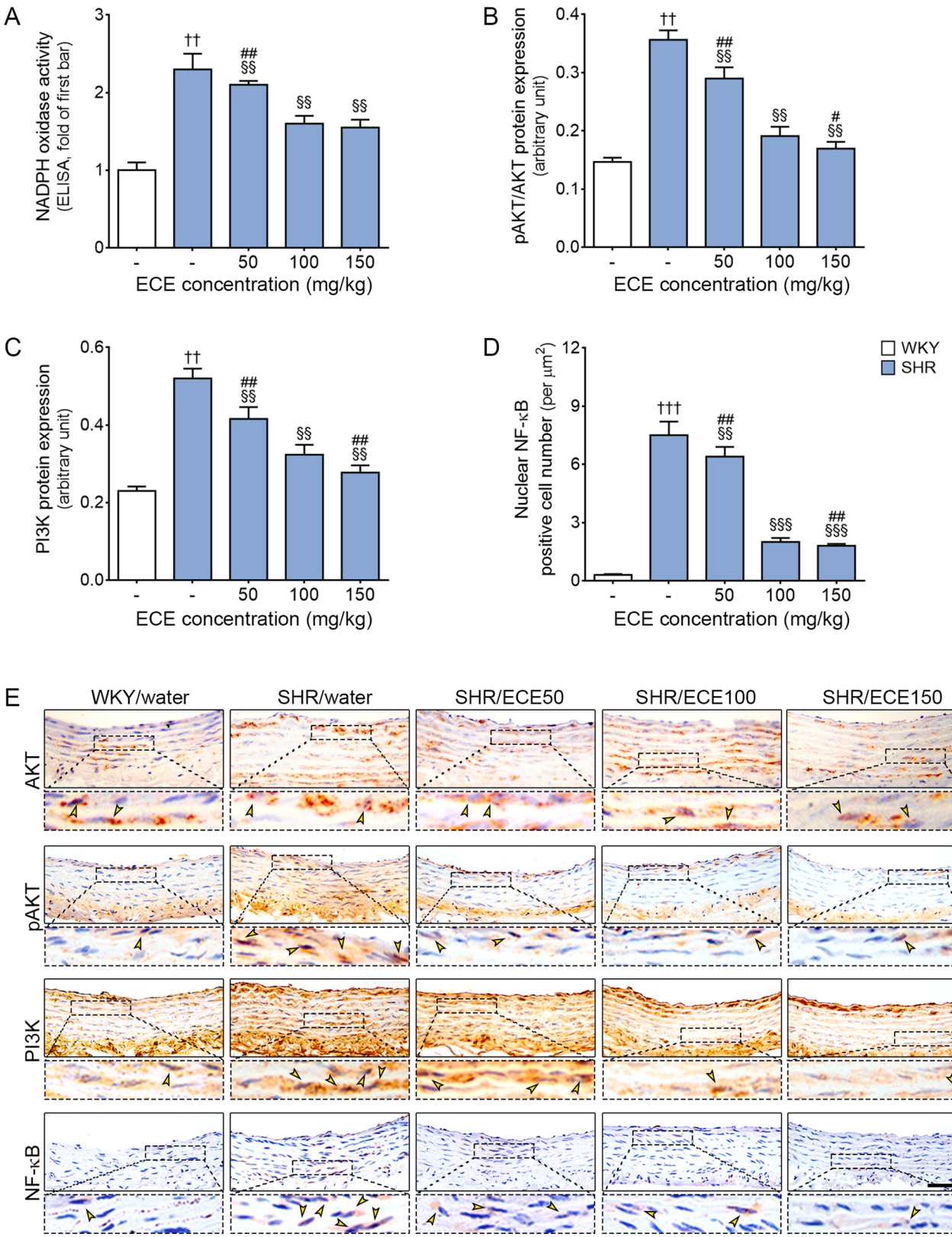

Fig. 5. Regulation of NADPH and PI3K/AKT and NF-κB expression by ECE treatment. (A) NADPH oxidase activity in the aortas of WKY, SHR, and SHR/ECEs was analyzed by ELISA. (B–D) The protein expression levels of pAKT/AKT (B), PI3K (C), and NF-κB (D) that developed in the medial layers of the animal aortas were quantified by Image J software after immunohistochemistry. (E) AKT, pAKT, PI3K and NF-κB expression in the aortas of WKY, SHR, and SHR/ECEs was analyzed by immunohistochemistry (scale bar = 100 μm). The yellow arrows represent positive signals. Data are presented as mean ± standard deviation. ††, $p < 0.01$, †††, $p < 0.001$ SHR/water vs. WKY/water; §§, $p < 0.01$, §§§, $p < 0.001$ SHR/ECEs vs. SHR/water; #, $p < 0.05$ ##, $p < 0.01$ SHR/ECEs vs. SHR/ECE100 (Mann–Whitney U test). AKT, protein kinase B; ECE, *Ecklonia cava* extract; NADPH, reduced nicotinamide adenine dinucleotide phosphate; NF-κB, nuclear factor kappa B; pAKT, phosphorylated AKT; PI3K, phosphoinositide 3-kinase; SHR, spontaneous hypertensive rat; WKY, Wistar Kyoto.

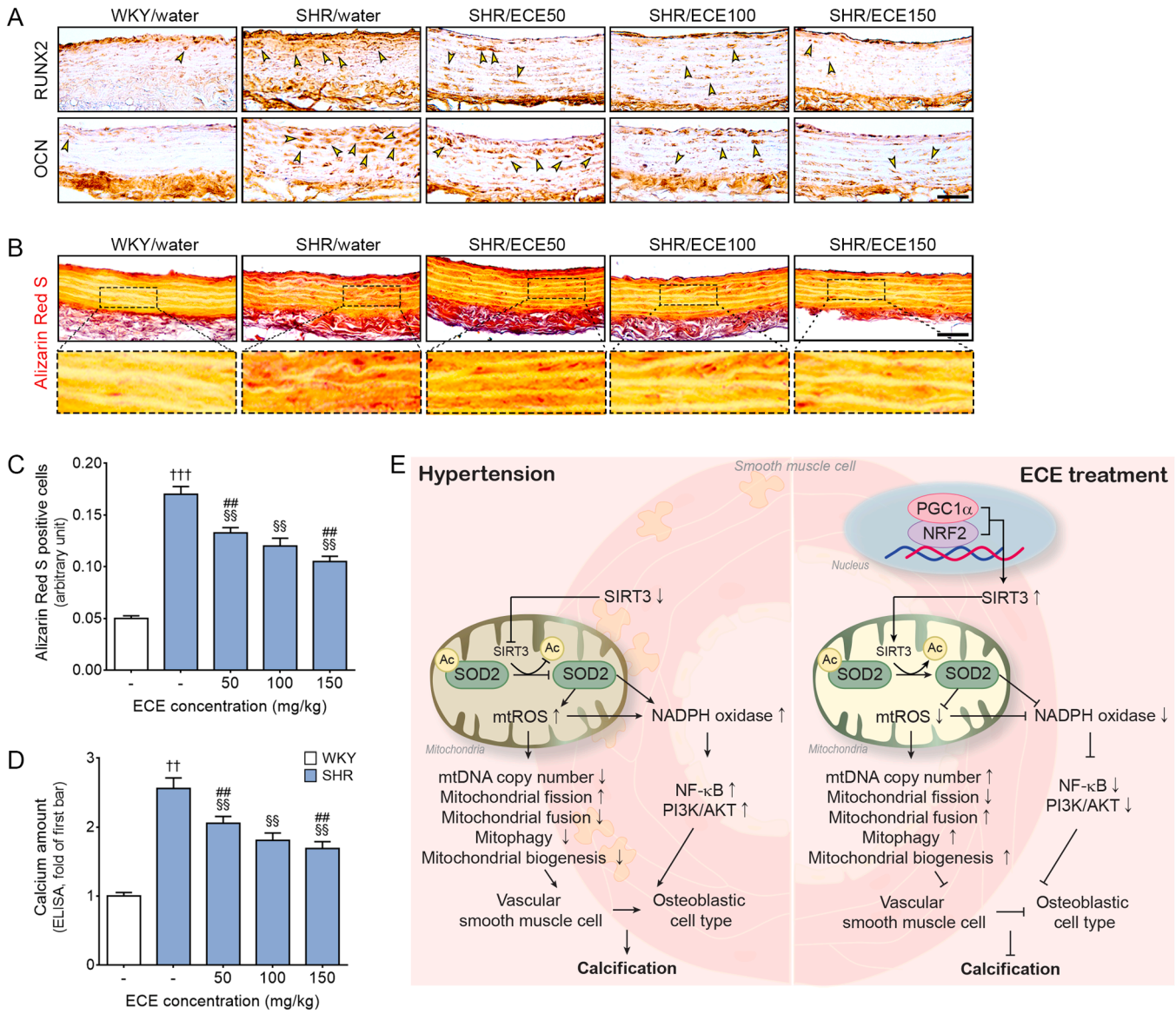

Fig. 6. Regulation of osteoblast-like VSMC changes and medial calcification by ECE treatment. (A) RUNX2 and OCN expression in the aortas of WKY, SHR, and SHR/ECEs were analyzed by immunohistochemistry. The yellow arrows represent positive signals (scale bar = 100 μm). (B) Amount of calcium deposition in the aortas of WKY, SHR, and SHR/ECEs was analyzed by indirect ELISA. The calcium deposition was increased in the SHR/water group and decreased after ECE treatment. (C and D) Calcium deposition in the aortas of WKY, SHR, and SHR/ECEs was determined by Alizarin Red S (scale bar = 100 μm). Alizarin Red S was positive in medial layer, with the high amount being observed in the SHR/water group and decreased after ECE treatment. (E) Figure shows the summary of this study. Data are presented as mean ± standard deviation. ††, $p < 0.01$, †††, $p < 0.001$ SHR/water vs. WKY/water; §§, $p < 0.01$ SHR/ECEs vs. SHR/water; ##, $p < 0.01$ SHR/ECEs vs. SHR/ECE100 (Mann–Whitney U test). Ac, acetyl; AKT, protein kinase B; ECE, *Ecklonia cava* extract; ELISA, enzyme-linked immunosorbent assay; mtDNA, mitochondrial deoxyribonucleic acid; NADPH, reduced nicotinamide adenine dinucleotide phosphate; NF-κB, nuclear factor kappa B; NRF2, nuclear factor erythroid 2-related factor 2; PGC-1α, peroxisome proliferator-activated receptor gamma coactivator-1 alpha; PI3K, phosphoinositide 3-kinase; OCN, osteocalcin; RUNX2, runt-related transcription factor 2; SHR, spontaneous hypertensive rat; SIRT3, sirtuin 3; SOD2, superoxide dismutase 2; WKY, Wistar Kyoto.

Mitochondrial fusion is also involved in the pathophysiology of VC [67,68]. Oxidized low-density lipoproteins are involved in OPA1 downregulation, which leads to the impairment of mitochondrial fusion and thus results in the development of atherosclerosis [69].

The increased mitochondrial fission by DRP1 leads to VC. DRP1 expression increases the calcification in the human carotid artery [70]. However, DRP1 deletion attenuates calcification in human valve interstitial cells and decreases VSMC migration. Pharmacological inhibition by the inhibitor of DRP1 leads to decreased calcification in H_2O_2-treated VSMCs [70]. Quercetin, an antioxidant, restores ROS-induced mitochondrial dysfunction and thus attenuates VC by decreasing mitochondrial fission via DRP1 inhibition [13].

Decreased mitochondrial biogenesis also leads to VC. Metformin attenuates the impairment of mitochondrial biogenesis by increasing AMPK activation and consequently decreases VC [71]. Mitochondrial biogenesis-related proteins, such as nuclear factor erythroid 2-related factor-1 (NRF-1) and PGC-1α, can also be upregulated by metformin treatment [71].

Our study showed that the expression of DRP1 and FIS1 (markers of mitochondrial fission) were increased in the SHR serum-treated MOVAS, and the expressions of both were decreased by ECE. However, the ECE's decreasing effect was not observed in the PGC-1α silencing MOVAS. OPA1 and MFN2 expressions were decreased by SHR serum and were increased by ECE. ECE's increasing effect was not observed in the PGC-1α silencing MOVAS. BNIP3 and ATG12 expression were decreased by the SHR serum and were increased by ECE. However, the increasing

effect was not observed in the PGC-1α silencing MOVAS. Expression of LC3II/LC3I was decreased by SHR serum and were increased by ECE. The increasing effect was eliminated by PGC-1α silencing. Expression of p62 was increased by SHR serum and were decreased by ECE. The increasing effect was eliminated by PGC-1α silencing. COX1 and SDHA expression were decreased by the SHR serum and were increased by ECE. However, those increasing effects were not observed in the PGC-1α silencing MOVAS. We also evaluated whether PGC-1α involved in effect of ECE on modulation of mitochondrial fission, fusion, mitophagy, and biogenesis through overexpression of PGC-1α. When overexpression of PGC-1α was induced, the SHR serum could not increase expression of DRP1, FIS1, P62 When overexpression of PGC-1α was induced, the SHR serum could not decrease expression of OPA1, MFN2, BNIP3, ATG12, LC3, COX1, SDHA, and mtDNA copy numbers. These results suggest that ECE decreases mitochondrial fission and increases mitochondrial fusion, mitophagy, and biogenesis via PGC-1α.

Furthermore, DRP1 and FIS1 expression in the aortic medial layer of SHR were increased and decreased dose-dependently due to ECE. OPA1 and MFN2 expression were decreased in the SHRs and increased by ECE. BNIP3, AGT2, COX1, and SDHA expression were decreased in the SHRs and were increased by ECE.

It is well known that mtROS accelerate the opening of the mitochondrial permeability transition pore (mPTP) and lead to release of mtROS into the cytosol, eventually activating the NADPH oxidase and inducing the formation of more cytosolic ROS [72,73].

Increased oxidative stress induced VSMC calcification via the PI3K/AKT/RUNX2 pathway [45]. Increased oxidative stress also leads to the upregulation of NF-κB/RUNX2 pathway and enhance vascular calcification [74].

In our study, NADPH oxidase activity was higher in the aortas of the SHRs than it was in the WKY rats but decreased after ECE treatment. In addition, PI3K, pAKT, and NF-κB expression were higher in the aortas of the SHRs than they were in the WKY rats and decreased by ECE. Osteoblast-like cell-type changes (evaluated with RUNX2 and OCN expression) as well as calcium deposition in the medial layer increased in the SHRs but decreased after ECE treatment.

Therefore, our study showed that ECE lead to decrease VC via the upregulation of PGC-1α and SIRT3, which increases SOD2 activity and decreases mtDNA damage and mtROS generation. However, our study had several limitations. Even though we evaluated various mitochondrial dysfunction markers by western blotting and tissue staining, we did not evaluate mitochondria morphology or number by Transmission electron microscopy which could provide most direct evidence of mitochondrial dysfunction. We performed silencing and overexpression of PGC-1α only in the in vitro model to evaluate whether ECE decreased VC via PGC-1α. To get more decisive evidence whether PGC-1α is main cell signaling pathway on decreasing VC by ECE, PGC-1α knock out animal model or overexpression animal model of PGC-1α should be used.

VC is associated with decreasing the elasticity and increasing the stiffness of the artery wall, and these changes lead to increased pulse wave velocity and the widening of the pulse pressure, which consequently contribute to the development of hypertension [75–77]. Severe arterial calcification frequently manifests in patients with resistant hypertension [78]. Moreover, VC manifests in 80% of patients with vascular injury and in 90% of patients with coronary artery disease. VC is a predictive factor for poor clinical outcomes in coronary atherosclerotic diseases [79]. Even though VC is related to increased mortality in cardiovascular diseases, effective therapies for VC have not been developed. Since the pathophysiology of VC is multifactorial, it is hard to find therapies for VC that could effectively inhibit the development of the VC pathway. The main pathophysiology of VC has been the result of increased ROS and mitochondrial dysfunction, which trigger the inflammation pathway. Thus, various natural or non-natural antioxidative compounds were tested to decrease VC [80].

ECE has been used as a food supplement and has been shown to be safe [81]. In our study, ECE modulated various signal pathways that are known to enhance VC by increasing mtROS, mt DNA damage, and mitochondrial dysfunction. Thus, it seems that ECE could be a potential therapy for VC which could be safely used.

In conclusion, ECE decreases VC by increasing the PGC-1α/NRF2/SIRT3 pathway and SIRT3 expression, which leads to increased SOD2 deacetylation. Activated SOD2 decreases mtDNA damage and mtROS generation, which sequentially decreases NADPH oxidase activity and changes in mitochondrial dynamics, thereby decreasing phenotype change of VSMCs to osteoblast-like cells and calcium deposition on the medial layer of the aorta.

Funding

This research was supported by Korea Institute of Marine Science & Technology Promotion(KIMST) funded by the Ministry of Oceans and Fisheries(2017-0285).

CRediT authorship contribution statement

Kyung-A Byun: Conceptualization, Methodology, Software, Formal analysis, Investigation, Data curation, Writing – original draft, Visualization. **Seyeon Oh:** Methodology, Software, Validation, Formal analysis, Data curation, Writing – review & editing. **Jin Young Yang:** Methodology, Validation, Data curation. **Soyoung Lee:** Software, Validation, Formal analysis. **Kuk Hui Son:** Conceptualization, Investigation, Writing – original draft, Writing – review & editing, Supervision, Project administration. **Kyunghee Byun:** Conceptualization, Investigation, Writing – original draft, Writing – review & editing, Supervision, Project administration, Funding acquisition.

Institutional review board statement

The study was conducted according to the guidelines of the Declaration of Helsinki and approved by the Institutional Animal Care and Use Committee of Gachon University (approval no. LCDI-2019-0121).

Data Availability

All data supporting the conclusions of this article are included in this article.

Acknowledgments

The authors would like to thank Aqua Green Technology Co., Ltd. (Jeju, South Korea), for the assistance in preparing ECE.

Conflicts of interest

The authors declare no conflicts of interest.

Appendix A. Supporting information

Supplementary data associated with this article can be found in the online version at doi:10.1016/j.biopha.2022.113283.

References

[1] M. Wu, C. Rementer, C.M. Giachelli, Vascular calcification: an update on mechanisms and challenges in treatment, Calcif. Tissue Int. 93 (2013) 365–373, https://doi.org/10.1007/s00223-013-9712-z.
[2] C.M. Giachelli, Vascular calcification mechanisms, J. Am. Soc. Nephrol. 15 (2004) 2959–2964, https://doi.org/10.1097/01.ASN.0000145894.57533.C4.
[3] N.D. Toussaint, P.G. Kerr, Vascular calcification and arterial stiffness in chronic kidney disease: implications and management, Nephrology 12 (2007) 500–509, https://doi.org/10.1111/j.1440-1797.2007.00823.x.

[4] S. Baktiroglu, F. Yanar, I.H. Ozata, G. Oner, D. Ercan, Arterial disease and vascular access in diabetic patients, J. Vasc. Access. 17 (2016) S69–S71, https://doi.org/10.5301/jva.5000532.

[5] X. Zhang, Y. Li, P. Yang, et al., Trimethylamine-N-oxide promotes vascular calcification through activation of NLRP3 (Nucleotide-Binding Domain, leucine-rich-containing family, Pyrin Domain-Containing-3) inflammasome and NF-κB (Nuclear Factor κB) Signals, Arterioscler. Thromb. Vasc. Biol. 40 (2020) 751–765, https://doi.org/10.1161/ATVBAHA.119.313414.

[6] H. Kim, H.J. Kim, K. Lee, et al., α-Lipoic acid attenuates vascular calcification via reversal of mitochondrial function and restoration of Gas6/Axl/Akt survival pathway, J. Cell. Mol. Med. 16 (2012) 273–286, https://doi.org/10.1111/j.1582-4934.2011.01294.x.

[7] L. Cui, Y. Bai, J. Zhang, S. Zhang, J. Xu, Effects of extracellular acid stimulation on rat vascular smooth muscle cell in Gas6/Axl or PI3K/Akt signaling pathway, Clin. Exp. Hypertens. 38 (2016) 451–456, https://doi.org/10.3109/10641963.2016.1163366.

[8] K.A. Hruska, S. Mathew, G. Saab, Bone morphogenetic proteins in vascular calcification, Circ. Res. 97 (2005) 105–114, https://doi.org/10.1161/01.RES.00000175571.53833.6c.

[9] P. Ducy, R. Zhang, V. Geoffroy, A.L. Ridall, G. Karsenty, Osf2/Cbfa1: a transcriptional activator of osteoblast differentiation, Cell 89 (1997) 747–754, https://doi.org/10.1016/s0092-8674(00)80257-3.

[10] K. Nakashima, X. Zhou, G. Kunkel, et al., The novel zinc finger-containing transcription factor osterix is required for osteoblast differentiation and bone formation, Cell 108 (2002) 17–29, https://doi.org/10.1016/s0092-8674(01)00622-5.

[11] T. Matsubara, K. Kida, A. Yamaguchi, et al., BMP2 regulates Osterix through Msx2 and Runx2 during osteoblast differentiation, J. Biol. Chem. 283 (2008) 29119–29125, https://doi.org/10.1074/jbc.M801774200.

[12] E. Bartolák-Suki, B. Suki, Tuning mitochondrial structure and function to criticality by fluctuation-driven mechanotransduction, Sci. Rep. 10 (2020) 407, https://doi.org/10.1038/s41598-019-57301-1.

[13] L. Cui, Z. Li, X. Chang, G. Cong, L. Hao, Quercetin attenuates vascular calcification by inhibiting oxidative stress and mitochondrial fission, Vasc. Pharmacol. 88 (2017) 21–29, https://doi.org/10.1016/j.vph.2016.11.006.

[14] S. van der Rijt, M. Molenaars, R.L. McIntyre, G.E. Janssens, R.H. Houtkooper, Integrating the hallmarks of aging throughout the tree of life: a focus on mitochondrial dysfunction, Front. Cell. Dev. Biol. 8 (2020), 594416, https://doi.org/10.3389/fcell.2020.594416.

[15] E.H. Sarsour, A.L. Kalen, P.C. Goswami, Manganese superoxide dismutase regulates a redox cycle within the cell cycle, Antioxid. Redox Signal. 20 (2014) 1618–1627, https://doi.org/10.1089/ars.2013.5303.

[16] I. Fridovich, Superoxide radical and superoxide dismutases, Annu. Rev. Biochem. 64 (1995) 97–112, https://doi.org/10.1146/annurev.bi.64.070195.000525.

[17] A.E. Dikalova, H.A. Itani, R.R. Nazarewicz, et al., Sirt3 impairment and SOD2 hyperacetylation in vascular oxidative stress and hypertension, Circ. Res. 121 (2017) 564–574, https://doi.org/10.1161/CIRCRESAHA.117.310933.

[18] R. Tao, A. Vassilopoulos, L. Parisiadou, Y. Yan, D. Gius, Regulation of MnSOD enzymatic activity by Sirt3 connects the mitochondrial acetylome signaling networks to aging and carcinogenesis, Antioxid. Redox Signal. 20 (2014) 1646–1654, https://doi.org/10.1089/ars.2013.5482.

[19] S. Winnik, J. Auwerx, D.A. Sinclair, C.M. Matter, Protective effects of sirtuins in cardiovascular diseases: from bench to bedside, Eur. Heart J. 36 (2015) 3404–3412, https://doi.org/10.1093/eurheartj/ehv290.

[20] H. Feng, J.Y. Wang, B. Yu, et al., Peroxisome proliferator-activated receptor-γ coactivator-1α inhibits vascular calcification through sirtuin 3-mediated reduction of mitochondrial oxidative stress, Antioxid. Redox Signal. 31 (2019) 75–91, https://doi.org/10.1089/ars.2018.7620.

[21] A. Qu, C. Jiang, M. Xu, et al., PGC-1alpha attenuates neointimal formation via inhibition of vascular smooth muscle cell migration in the injured rat carotid artery, Am. J. Physiol. Cell. Physiol. 297 (2009) C645–C653, https://doi.org/10.1152/ajpcell.00469.2008.

[22] A.D. Cherry, H.B. Suliman, R.R. Bartz, C.A. Piantadosi, Peroxisome proliferator-activated receptor γ co-activator 1-α as a critical co-activator of the murine hepatic oxidative stress response and mitochondrial biogenesis in Staphylococcus aureus sepsis, J. Biol. Chem. 289 (2014) 41–52, https://doi.org/10.1074/jbc.M113.512483.

[23] J. St-Pierre, S. Drori, M. Uldry, et al., Suppression of reactive oxygen species and neurodegeneration by the PGC-1 transcriptional coactivators, Cell 127 (2006) 397–408, https://doi.org/10.1016/j.cell.2006.09.024.

[24] B.N. Finck, D.P. Kelly, PGC-1 coactivators: inducible regulators of energy metabolism in health and disease, J. Clin. Invest. 116 (2006) 615–622, https://doi.org/10.1172/JCI27794.

[25] N. Gleyzer, K. Vercauteren, R.C. Scarpulla, Control of mitochondrial transcription specificity factors (TFB1M and TFB2M) by nuclear respiratory factors (NRF-1 and NRF-2) and PGC-1 family coactivators, Mol. Cell. Biol. 25 (2005) 1354–1366, https://doi.org/10.1128/MCB.25.4.1354-1366.2005.

[26] C. Song, B. Fu, J. Zhang, et al., Sodium fluoride induces nephrotoxicity via oxidative stress-regulated mitochondrial SIRT3 signaling pathway, Sci. Rep. 7 (2017) 672, https://doi.org/10.1038/s41598-017-00796-3.

[27] M.M. Kim, Q.V. Ta, E. Mendis, et al., Phlorotannins in Ecklonia cava extract inhibit matrix metalloproteinase activity, Life. Sci. 79 (2006) 1436–1443, https://doi.org/10.1016/j.lfs.2006.04.022.

[28] S. Oh, M. Son, J. Choi, et al., Phlorotannins from Ecklonia cava attenuates palmitate-induced endoplasmic reticulum stress and leptin resistance in hypothalamic neurons, Mar. Drugs 17 (2019) 570, https://doi.org/10.3390/md17100570.

[29] M. Son, S. Oh, J.T. Jang, K.H. Son, K. Byun, Pyrogallol-phloroglucinol-6 6-bieckol on attenuates high-fat diet-induced hypertension by modulating endothelial-to-mesenchymal transition in the aorta of mice, Oxid. Med. Cell. Longev. 2021 (2021), 8869085, https://doi.org/10.1155/2021/8869085.

[30] H. Eo, J.E. Park, Y.J. Jeon, Y. Lim, Ameliorative effect of Ecklonia cava polyphenol extract on renal inflammation associated with aberrant energy metabolism and oxidative stress in high fat diet-induced obese mice, J. Agric. Food Chem. 65 (2017) 3811–3818, https://doi.org/10.1021/acs.jafc.7b00357.

[31] M. Son, S. Oh, H.S. Lee, et al., Ecklonia cava extract attenuates endothelial cell dysfunction by modulation of inflammation and brown adipocyte function in perivascular fat tissue, Nutrients 11 (2019) 2795, https://doi.org/10.3390/nu11112795.

[32] A.R. Crowe, W. Yue, Semi-quantitative determination of protein expression using immunohistochemistry staining and analysis: an integrated protocol, Bio Protoc. 9 (2019), e3465, https://doi.org/10.21769/BioProtoc.3465.

[33] X. Li, X. Wang, M. Zheng, Q.X. Luan, Mitochondrial reactive oxygen species mediate the lipopolysaccharide-induced pro-inflammatory response in human gingival fibroblasts, Exp. Cell. Res. 347 (2016) 212–221, https://doi.org/10.1016/j.yexcr.2016.08.007.

[34] F. Cividini, B.T. Scott, A. Dai, et al., O-GlcNAcylation of 8-oxoguanine DNA glycosylase (Ogg1) impairs oxidative mitochondrial DNA lesion repair in diabetic hearts, J. Biol. Chem. 291 (2016) 26515–26528, https://doi.org/10.1074/jbc.M116.754481.

[35] Y.L. He, S.H. Gong, X. Cheng, et al., BNIP3 phosphorylation by JNK1/2 promotes mitophagy via enhancing its stability under hypoxia, BioRxiv (2020), https://doi.org/10.1101/2020.08.27.271270.

[36] C.T. Chu, J. Zhu, R. Dagda, Beclin 1-independent pathway of damage-induced mitophagy and autophagic stress: implications for neurodegeneration and cell death, Autophagy 3 (2007) 663–666, https://doi.org/10.4161/auto.4625.

[37] T. Zhang, L. Xue, L. Li, et al., BNIP3 protein suppresses PINK1 kinase proteolytic cleavage to promote mitophagy, J. Biol. Chem. 291 (2016) 21616–21629, https://doi.org/10.1074/jbc.M116.733410.

[38] J. Gao, S. Qin, C. Jiang, Parkin-induced ubiquitination of Mff promotes its association with p62/SQSTM1 during mitochondrial depolarization, Acta Biochim. Biophys. Sin. 47 (2015) 522–529, https://doi.org/10.1093/abbs/gmv044.

[39] J. Augustyniak, J. Lenart, M. Zychowicz, et al., Mitochondrial biogenesis and neural differentiation of human iPSC is modu-lated by idebenone in a developmental stage-dependent manner, Biogerontology 18 (2017) 665–677, https://doi.org/10.1007/s10522-017-9718-4.

[40] F. Cioffi, A. Giacco, G. Petito, et al., Altered mitochondrial quality control in rats with metabolic dysfunction-associated fatty liver disease (MAFLD) induced by high-fat feeding, Genes 13 (2022) 315, https://doi.org/10.3390/genes13020315.

[41] D. Zhu, N.C. Mackenzie, J.L. Millán, C. Farquharson, V.E. MacRae, The appearance and modulation of osteocyte marker expression during calcification of vascular smooth muscle cells, PLoS One 6 (2011), e19595, https://doi.org/10.1371/journal.pone.0019595.

[42] S. Jono, M.D. McKee, C.E. Murry, et al., Phosphate regulation of vascular smooth muscle cell calcification, Circ. Res. 87 (2000) E10–E17, https://doi.org/10.1161/01.res.87.7.e10.

[43] R. Villa-Bellosta, Dietary magnesium supplementation improves lifespan in a mouse model of progeria, EMBO Mol. Med 12 (2020), e12423, https://doi.org/10.15252/emmm.202012423.

[44] J. He, X. Liu, C. Su, et al., Inhibition of mitochondrial oxidative damage improves reendothelialization capacity of endothelial progenitor cells via SIRT3 (Sirtuin 3)-Enhanced SOD2 (Superoxide Dismutase 2) deacetylation in hypertension, Arterioscler. Thromb. Vasc. Biol. 39 (2019) 1682–1698, https://doi.org/10.1161/ATVBAHA.119.312613.

[45] C.H. Byon, A. Javed, Q. Dai, et al., Oxidative stress induces vascular calcification through modulation of the osteogenic transcription factor Runx2 by AKT signaling, J. Biol. Chem. 283 (2008) 15319–15327, https://doi.org/10.1074/jbc.M800021200.

[46] C.H. Byon, J.M. Heath, Y. Chen, Redox signaling in cardiovascular pathophysiology: a focus on hydrogen peroxide and vascular smooth muscle cells, Redox Biol. 9 (2016) 244–253, https://doi.org/10.1016/j.redox.2016.08.015.

[47] P. Wang, N. Zhang, B. Wu, S. Wu, Y. Zhang, Y. Sun, The role of mitochondria in vascular calcification, J. Transl. Int. Med. 8 (2020) 80–90, https://doi.org/10.2478/jtim-2020-0013.

[48] K. Okamoto, Establishment of the stroke-prone spontaneously hypertensive rat (SHR), Circ. Res. 34 (1974) 143–153.

[49] M. Majzunova, M. Kvandova, A. Berenyiova, et al., Chronic NOS inhibition affects oxidative state and antioxidant re-sponse differently in the kidneys of young normotensive and hypertensive rats, Oxid. Med. Cell Longev. 2019 (2019), 5349398, https://doi.org/10.1155/2019/5349398.

[50] H. Wang, H. Jiang, H. Liu, et al., Modeling disease progression: angiotensin II indirectly inhibits nitric oxide production via ADMA accumulation in spontaneously hypertensive rats, Front Physiol. 7 (2016) 555, https://doi.org/10.3389/fphys.2016.00555.

[51] Cantó, Z. Gerhart-Hines, J.N. Feige, et al., AMPK regulates energy expenditure by modulating NAD+ metabolism and SIRT1 activity, Nature 458 (2009) 1056–1060, https://doi.org/10.1038/nature07813.

[52] T. Fukai, M. Ushio-Fukai, Superoxide dismutases: role in redox signaling, vascular function, and diseases, Antioxid. Redox Signal. 15 (2011) 1583–1606, https://doi.org/10.1089/ars.2011.3999.

[53] A.M. Markin, V.A. Khotina, X.G. Zabudskaya, et al., Disturbance of mitochondrial dynamics and mitochondrial therapies in atherosclerosis, Life 11 (2021) 165, https://doi.org/10.3390/life11020165.
[54] Y.M. Kim, S.W. Youn, V. Sudhahar, et al., Redox regulation of mitochondrial fission protein Drp1 by protein disulfide isomerase limits endothelial senescence, Cell. Rep. 23 (2018) 3565–3578, https://doi.org/10.1016/j.celrep.2018.05.054.
[55] S. Frank, B. Gaume, E.S. Bergmann-Leitner, et al., The role of dynamin-related protein 1, a mediator of mitochondrial fission, in apoptosis, Dev. Cell. 1 (2001) 515–525, https://doi.org/10.1016/s1534-5807(01)00055-7.
[56] D.I. James, P.A. Parone, Y. Mattenberger, J.C. Martinou, hFis1, a novel component of the mammalian mitochondrial fission machinery, J. Biol. Chem. 278 (2003) 36373–36379, https://doi.org/10.1074/jbc.M303758200.
[57] S. Gandre-Babbe, A.M. van der Bliek, The novel tail-anchored membrane protein Mff controls mitochondrial and peroxisomal fission in mammalian cells, Mol. Biol. Cell. 19 (2008) 2402–2412, https://doi.org/10.1091/mbc.e07-12-1287.
[58] A. Santel, S. Frank, B. Gaume, M. Herrler, R.J. Youle, M.T. Fuller, Mitofusin-1 protein is a generally expressed mediator of mitochondrial fusion in mammalian cells, J. Cell. Sci. 116 (2003) 2763–2774, https://doi.org/10.1242/jcs.00479.
[59] A. Santel, M.T. Fuller, Control of mitochondrial morphology by a human mitofusin, J. Cell. Sci. 114 (2001) 867–874.
[60] S. Cipolat, O. Martins de Brito, B. Dal Zilio, L. Scorrano, OPA1 requires mitofusin 1 to promote mitochondrial fusion, Proc. Natl. Acad. Sci U.S.A. 101 (2004) 15927–15932, https://doi.org/10.1073/pnas.0407043101.
[61] N. Burke, A.R. Hall, D.J. Hausenloy, OPA1 in cardiovascular health and disease, Curr. Drug. Targets 16 (2015) 912–920, https://doi.org/10.2174/1389450116666150102113648.
[62] G. Chandhok, M. Lazarou, B. Neumann, Structure, function, and regulation of mitofusin-2 in health and disease, Biol. Rev. Camb. Philos. Soc. 93 (2018) 933–949, https://doi.org/10.1111/brv.12378.
[63] Y. Zhang, Y. Wang, J. Xu, et al., Melatonin attenuates myocardial ischemia-reperfusion injury via improving mitochondrial fusion/mitophagy and activating the AMPK-OPA1 signaling pathways, J. Pineal Res. 66 (2019), e12542, https://doi.org/10.1111/jpi.12542.
[64] T. Saito, J. Sadoshima, Molecular mechanisms of mitochondrial autophagy/mitophagy in the heart, Circ. Res. 116 (2015) 1477–1490, https://doi.org/10.1161/CIRCRESAHA.116.303790.
[65] L. Liu, K. Sakakibara, Q. Chen, et al., Receptor-mediated mitophagy in yeast and mammalian systems, Cell Res. 24 (2014) 787–795, https://doi.org/10.1038/cr.2014.75.
[66] Y. Zhu, J.J. Ji, R. Yang, et al., Lactate accelerates calcification in VSMCs through suppression of BNIP3-mediated mitopha-gy, Cell Signal 58 (2019) 53–64, https://doi.org/10.1016/j.cellsig.2019.03.006.
[67] S.Y. Lee, C.T. Chao, J.W. Huang, K.C. Huang, Vascular calcification as an underrecognized risk factor for frailty in 1783 community-dwelling elderly individuals, J. Am. Heart Assoc. 9 (2020), e017308, https://doi.org/10.1161/JAHA.120.017308.
[68] J.R. Lewis, C.J. Eggermont, J.T. Schousboe, et al., Association between abdominal aortic calcification, bone mineral density, and fracture in older women, J. Bone Miner. Res. 34 (2019) 2052–2060, https://doi.org/10.1002/jbmr.3830.
[69] J. Zheng, C. Lu, Oxidized LDL causes endothelial apoptosis by inhibiting mitochondrial fusion and mitochondria autophagy, Front. Cell. Dev. Biol. 8 (2020), 600950, https://doi.org/10.3389/fcell.2020.600950.
[70] M.A. Rogers, N. Maldonado, J.D. Hutcheson, et al., Dynamin-related protein 1 inhibition attenuates cardiovascular calcification in the presence of oxidative stress, Circ. Res. 121 (2017) 220–233, https://doi.org/10.1161/CIRCRESAHA.116.310293.
[71] W.Q. Ma, X.J. Sun, Y. Wang, Y. Zhu, X.Q. Han, N.F. Liu, Restoring mitochondrial biogenesis with metformin attenuates β-GP-induced phenotypic transformation of VSMCs into an osteogenic phenotype via inhibition of PDK4/oxidative stress-mediated apoptosis, Mol. Cell. Endocrinol. 479 (2019) 39–53, https://doi.org/10.1016/j.mce.2018.08.012.
[72] S.I. Dikalov, R.R. Nazarewicz, A. Bikineyeva, et al., Nox2-induced production of mitochondrial superoxide in angiotensin II-mediated endothelial oxidative stress and hypertension, Antioxid. Redox Signal 20 (2014) 281–294, https://doi.org/10.1089/ars.2012.4918.
[73] S. Kröller-Schön, S. Steven, S. Kossmann, et al., Molecular mechanisms of the crosstalk between mitochondria and NADPH oxidase through reactive oxygen species-studies in white blood cells and in animal models, Antioxid. Redox Signal 20 (2014) 247–266, https://doi.org/10.1089/ars.2012.4953.
[74] M.M. Zhao, M.J. Xu, Y. Cai, et al., Mitochondrial reactive oxygen species promote p65 nuclear translocation mediating high-phosphate-induced vascular calcification in vitro and in vivo, Kidney Int. 79 (2011) 1071–1079, https://doi.org/10.1038/ki.2011.18.
[75] J. Blacher, A.P. Guerin, B. Pannier, S.J. Marchais, G.M. London, Arterial calcifications, arterial stiffness, and cardiovascular risk in end-stage renal disease, Hypertension 38 (2001) 938–942, https://doi.org/10.1161/hy1001.096358.
[76] N.D. Toussaint, K.K. Lau, B.J. Strauss, K.R. Polkinghorne, P.G. Kerr, Associations between vascular calcification, arterial stiffness and bone mineral density in chronic kidney disease, Nephrol. Dial. Transplant. 23 (2008) 586–593, https://doi.org/10.1093/ndt/gfm660.
[77] M. Temmar, S. Liabeuf, C. Renard, et al., Pulse wave velocity and vascular calcification at different stages of chronic kid-ney disease, J. Hypertens. 28 (2010) 163–169, https://doi.org/10.1097/HJH.0b013e328331b81e.
[78] C.M. McEniery, B.J. McDonnell, A. So, et al., Aortic calcification is associated with aortic stiffness and isolated systolic hy-pertension in healthy individuals, Hypertension 53 (2009) 524–531, https://doi.org/10.1161/HYPERTENSIONAHA.108.126615.
[79] K. Yahagi, F.D. Kolodgie, C. Lutter, et al., Pathology of human coronary and carotid artery atherosclerosis and vascular calcification in Diabetes Mellitus, Arterioscler. Thromb. Vasc. Biol. 37 (2017) 191–204, https://doi.org/10.1161/ATVBAHA.116.306256.
[80] C.T. Chao, H.Y. Yeh, Y.T. Tsai, et al., Natural and non-natural antioxidative compounds: potential candidates for treatment of vascular calcification, Cell Death Discov. 5 (2019) 145, https://doi.org/10.1038/s41420-019-0225-z.
[81] E.F.S.A. Panel on Dietetic Products, Nutrition and Allergies (NDA), D. Turck, J. L. Bresson, et al., Safety of Ecklonia cava phlo-rotannins as a novel food pursuant to Regulation (EC) No 258/97, EFSA J. 15 (2017), e05003, https://doi.org/10.2903/j.efsa.2017.5003.